JOURNAL OF MODERN OPTICS, 1990, VOL. 37, NO. 5, 889–917

Displaced and squeezed Fock states

P. KRÁL

Institute of Physics, Czechoslovak Academy of Science,
Na Slovance 2, 180 40 Praha 8, Czechoslovakia

(Received 16 June 1989; revision received 26 September 1989 and accepted 29 September 1989)

Abstract. Energy eigenstates of a quantum harmonic oscillator are displaced, squeezed and finally damped by one- and two-photon absorption process. Quantum fluctuations, quasi-distributions, photon-number statistics and wavefunctions are investigated for them both analytically and numerically. We propose new methods for analytic treatment.

1. Introduction

Displaced and squeezed vacuum states of a quantum mechanical light field have been produced in several laboratories [1]. This leads us to think over their applications [2] or more sophisticated generalizations [3]. Nowadays, the centre of attention concerns those states with reduced or extended quantum fluctuations in one or the other canonical component, in such a way that the Heisenberg uncertainty principle is preserved. A typical example is amplitude squeezed states or crescent states [4]. Another candidate are Fock states, having zero number uncertainty and promising hopeful applications in communications and spectroscopy. Several methods for their production and jump-like amplification have been suggested [5] and the first Fock state has already been observed [6]. However an experimental observation of higher Fock states is still in the future. Our problem is what happens with Fock states when they are displaced and squeezed?

The paper is organized as follows. In section 2 we review a few concepts concerning a coherent and squeezed vacuum and extend them to the Fock states. We also present quantum fluctuations for these states. In section 3 we derive quasi-distributions, photon-number distributions and some of the wavefunctions. Section 4 is devoted to a solution of a degenerate parametric amplification process with classical pumping for a displaced Fock state as the input. In section 5 we use the one-parametric anti-normal quasi-distribution, found in section 4, as the input of a single-mode system and an infinite phonon reservoir in the Markoff approximation. From the damped antinormal characteristic function found here we derive various features of damped states in two limits $\beta=0$, $\nu=0$. In section 6 we present numerical examples and explain their mutual connection. The conclusion completes the paper from other points of view.

2. Coherent and squeezed states, quantum fluctuations of $|\beta, m\rangle_g$

A more thorough description of squeezed states can be found in Yuen's paper [8], from which we take a few necessary definitions and results.

Coherent states $|\alpha\rangle$ result in evolution of the vacuum state $|0\rangle$ at the action of the unitary operator $D(\alpha)$. They satisfy

$$a|\alpha\rangle = aD(\alpha)|0\rangle = \alpha|\alpha\rangle, \tag{2.1}$$

where a is the anihilation operator and

$$D(\alpha) = \exp(\alpha a^+ - \alpha^* a). \tag{2.2}$$

Similarly, squeezed states $|\beta\rangle_g$ (TCSs) resulting in application of the unitary operator $S(\zeta)$ on $|\beta\rangle$ have the properties

$$b|\beta\rangle_g = bS(\zeta)|\beta\rangle = \beta|\beta\rangle_g, \tag{2.3}$$

where

$$b = \mu a + \nu a^+, \qquad \beta = \mu\alpha_0 + \nu\alpha_0^*, \tag{2.4}$$

$$S(\zeta) = \exp(\zeta a^{+2} - \zeta^* a^2). \tag{2.5}$$

The parameters α_0 and α_0^* represent equivalent shift of a squeezed vacuum, as is obvious from (2.10). ζ and ζ^* are related to μ and ν by [9]

$$\mu = \cosh(r), \qquad \nu = \exp(-i\theta)\sinh(r), \qquad \zeta = -(r/2)\exp(-i\theta), \tag{2.6}$$

where for μ and ν it holds that

$$|\mu|^2 - |\nu|^2 = 1. \tag{2.7}$$

Displacing and squeezing operators transform a and a^+ according to well known relations [9]

$$D(\alpha)aD^+(\alpha) = a - \alpha, \qquad D(\alpha)a^+D^+(\alpha) = a^+ - \alpha^*, \tag{2.8}$$

$$S(\zeta)aS^+(\zeta) = \mu a + \nu a^+ = b, \qquad S(\zeta)a^+S^+(\zeta) = \mu^* a^+ + \nu^* a = b^+. \tag{2.9}$$

By applying (2.9) to the operator $D(\beta)$ appearing in $|\beta\rangle_g$ we easily obtain

$$S(\zeta)|\beta\rangle = S(\zeta)D(\beta)|0\rangle = D(\alpha_0)S(\zeta)|0\rangle, \tag{2.10}$$

where α_0, α_0^* are related with β, β^* through (2.4).

After these preliminaries we can define displaced and squeezed Fock states by the formula [9]

$$|\beta, m\rangle_g = S(\zeta)D(\beta)|m\rangle = S(\zeta)D(\beta)\frac{a^{+m}}{\sqrt{m!}}|0\rangle. \tag{2.11}$$

Let us investigate several moments of the field $|\beta, m\rangle_g$. We need to transform (2.4) and its adjoint as follows

$$a = \mu^* b - \nu b^+, \qquad a^+ = \mu b^+ - \nu^* b. \tag{2.12}$$

Making use of (2.12, 8, 9), we at once obtain

$$\langle a\rangle = \langle a^+\rangle^* = \langle m|D^+(\beta)S^+(\zeta)aS(\zeta)D(\beta)|m\rangle = \mu^*\beta - \nu\beta^* = \alpha_0, \tag{2.13}$$

$$\langle a^2\rangle = \langle a^{+2}\rangle^* = \alpha_0^2 - \mu^*\nu(2m+1), \tag{2.14}$$

$$\langle n\rangle = \langle a^+ a\rangle = (|\mu|^2 + |\nu|^2)m + |\nu|^2 + |\alpha_0|^2, \tag{2.15}$$

$$\langle \Delta^2 n\rangle = \langle n^2\rangle - \langle n\rangle^2 = |\alpha_0\mu - \alpha_0^*\nu|^2(2m+1) + 2|\mu\nu|^2(m^2+m+1). \tag{2.16}$$

Sub-Poissonian behaviour of the states $|\beta, m\rangle_g$ can be investigated from the ratio of (2.16) to (2.15). We denote $r=\langle\Delta^2 n\rangle/\langle n\rangle$ and remark that the inequality $r<1$ just holds for a sub-Poissonian light. Two separate cases follow. One corresponds to the coordinate centre located inside the ring-like ϕ_{ss} (see section 3). For a large m both the first term in (2.15) and the last term in (2.16) can dominate. The condition $r<1$ then gives the inequality $2|\mu v|^2 m<1$, which limits the magnitude of v. The second case of $r<1$ is when the coordinate centre lies outside ϕ_{ss}. Then both the last term in (2.15) and the first term in (2.16) can prevail and phase conditions of the term in absolute value in (2.16), determine the magnitude of r. We will not pursue other cases, when more terms in (2.15) or (2.16) are comparable.

To discuss squeezing of displaced and squeezed Fock states we employ the definition of canonical coordinate operators q, p with $\omega=1$,

$$q=(\hbar/2)^{1/2}(a^+ +a), \qquad p=\mathrm{i}(\hbar/2)^{1/2}(a^+ -a), \tag{2.17}$$

and find that

$$\left\langle\left(\Delta\begin{matrix}q\\p\end{matrix}\right)^2\right\rangle=(\hbar/2)(2m+1)|\mu\mp v|^2, \tag{2.18}$$

$$\langle\Delta^2 q\rangle\langle\Delta^2 p\rangle=(\hbar^2/4)(2m+1)^2, \tag{2.19}$$

$$\det\sigma=\sigma_{pp}\sigma_{qq}-\sigma_{pq}^2=(\hbar^2/4)(2m+1)^2\{|\mu^2-v^2|^2+4[\mathrm{Im}\,(\mu v^*)]^2\}, \tag{2.20}$$

where [9]

$$\sigma_{ij}=\langle(\tfrac{1}{2})(ij+ji)-\langle i\rangle\langle j\rangle\rangle.$$

We can observe that squeezing properties related to $|\beta, m\rangle_g$ states can be directly deduced from those for the displaced and squeezed vacuum $|\beta\rangle_g$, with the change of $\hbar/2$ to $(\hbar/2)(2m+1)$. From (2.18, 19) it is further evident that for every m the state $|\beta, m\rangle_g$ may have, under appropriate values of μ, v, one of the quadrature variances less than $\hbar/2$, corresponding to a coherent state.

We can adopt the concept of principal squeezing [10] to $|\beta, m\rangle_g$ particularly. By denoting λ_1 or λ_2 a large, or small half-axis of a noise ellipse representing squeezed quadrature fluctuations [11], we can say that these states are principally squeezed if $\lambda_2<(2m+1)$. If $\lambda_2<1$ they are principally squeezed below the vacuum. Here we employ the term of squeezing whenever the half-axes are different. From (2.19) it follows that

$$\lambda_1\lambda_2=(2m+1)^2, \tag{2.21}$$

which refers to the fact that quantum fluctuations in one quadrature increase according to the detriment of those from the conjugate quadrature.

3. Quasi-distributions, photon-number distributions and wavefunctions

Let us briefly recapitulate some known definitions [7]. Anti-normal quasi-distribution ϕ_{ss} is related with the corresponding density operator ρ and the normal quasi-distribution ϕ_N,

$$\phi_{ss}(\alpha)=\langle\alpha|\rho|\alpha\rangle/\pi=\int\phi_N(\beta)\exp(-|\alpha-\beta|^2)\,\mathrm{d}^2\beta. \tag{3.1}$$

Anti-normal or normal characteristic functions are defined as

$$C_{\mathscr{A}}(\beta)=\mathrm{Tr}\{\rho\exp(-\beta^*a)\exp(\beta a^+)\}=\int\phi_{\mathscr{A}}(\alpha)\exp(\beta\alpha^*-\beta^*\alpha)\,\mathrm{d}^2\alpha, \tag{3.2}$$

$$C_{\mathscr{N}}(\beta)=\mathrm{Tr}\{\rho\exp(\beta a^+)\exp(-\beta^*a)\}=\int\phi_{\mathscr{N}}(\alpha)\exp(\beta\alpha^*-\beta^*\alpha)\,\mathrm{d}^2\alpha. \tag{3.3}$$

They are mutually related with the symmetric characteristic function as follows:

$$C_{\mathscr{N}}(\beta)=\exp(|\beta|^2/2)\,C_{\mathscr{S}}(\beta)=\exp(|\beta|^2)\,C_{\mathscr{A}}(\beta). \tag{3.4}$$

The corresponding quasi-distributions are the inverse Fourier transforms

$$\phi_{\mathscr{N},\mathscr{A},\mathscr{S}}(\alpha)=\frac{1}{\pi^2}\int C_{\mathscr{N},\mathscr{A},\mathscr{S}}(\beta)\exp(\alpha\beta^*-\alpha^*\beta)\,\mathrm{d}^2\beta. \tag{3.5}$$

The photon-number normal characteristic function is simply connected to these quantities and can be computed [7],

$$C_{\mathscr{N}}^{(w)}(\lambda)=\frac{1}{\pi\lambda}\int\exp\left(-\frac{|\beta|^2}{\lambda}\right)C_{\mathscr{N}}(\beta)\,\mathrm{d}^2\beta. \tag{3.6}$$

Characteristic functions generate photon-number distributions and various moments through

$$p(n)=\frac{(-1)^n}{n!}\frac{\mathrm{d}^n}{\mathrm{d}\lambda^n}C_{\mathscr{N}}^{(w)}(\lambda)\bigg|_{\lambda=1}, \tag{3.7}$$

$$\langle W^k\rangle_{\mathscr{N}}=(-1)^k\frac{\mathrm{d}^k}{\mathrm{d}\lambda^k}C_{\mathscr{N}}^{(w)}(\lambda)\bigg|_{\lambda=0}, \tag{3.8}$$

$$\left\langle\begin{matrix}\mathscr{N}\\ \mathscr{A}\end{matrix}(\alpha^{*k}\alpha^l)\right\rangle=\frac{\partial^k}{\partial\beta^k}\frac{\partial^l}{\partial(-\beta^*)^l}C_{\mathscr{N},\mathscr{A}}(\beta,\beta^*)\bigg|_{\beta=\beta^*=0}, \tag{3.9}$$

where $\mathscr{N}$ and $\mathscr{A}$ denote the normal and anti-normal ordering operators respectively [12].

To deduce $\phi_{\mathscr{A}}(\alpha)$ for the field $|\beta,m\rangle_g$, we employ techniques derived from methods of generating functions (see [17]). We insert the factor $\exp(\lambda a^+)$ inside the matrix element $\langle\alpha|\beta\rangle_g$ found in [8] and as a result obtain $\langle\alpha|\beta,m\rangle_g$ (see Appendix),

$$\langle\alpha|S(\zeta)D(\beta)|m\rangle=\frac{1}{\sqrt{m!}}\left(\frac{-v^*}{2\mu}\right)^{m/2}H_m\left(\frac{\alpha^*-\alpha_0^*}{(-2\mu v^*)^{1/2}}\right)\langle\alpha|\beta\rangle_g. \tag{3.10}$$

So that $\phi_{\mathscr{A}}^m$ gets the following form

$$\phi_{\mathscr{A}}^m(\alpha)=\frac{1}{\pi m!}|v^*/2\mu|^m\left|H_m\left(\frac{\alpha^*-\alpha_0^*}{(-2\mu v^*)^{1/2}}\right)\right|^2|\langle\alpha|\beta\rangle_g|^2, \tag{3.11}$$

having for $v\to0$ the correct limit of $\phi_{\mathscr{A}}^m$ for displaced Fock states [7]

$$\phi_{\mathscr{A}}^m(\alpha)=\frac{1}{\pi m!}|\alpha-\alpha_0|^{2m}\exp(-|\alpha-\alpha_0|^2). \tag{3.12}$$

In figure 1 we demonstrate several examples of the evolution of $\phi_{\mathscr{A}}^2$ for $|0,2\rangle_g$, where $v=0,0{\cdot}5,1,2$. The circle-like $\phi_{\mathscr{A}}$ for the Fock state first becomes eliptic, as we

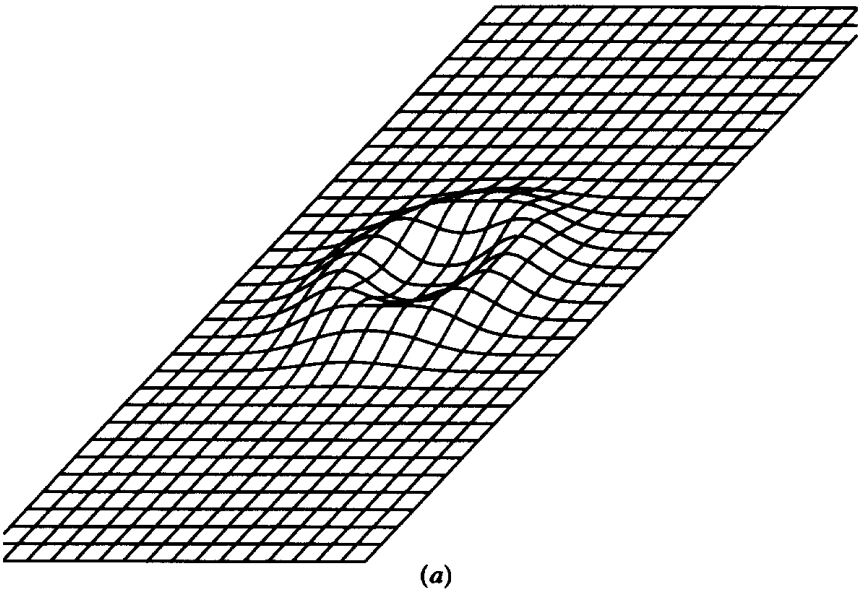

(*a*)

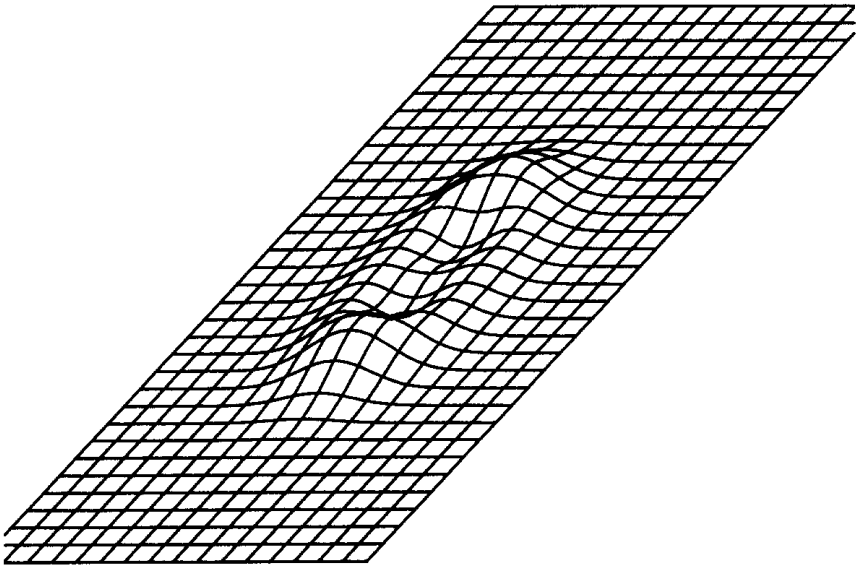

(*b*)

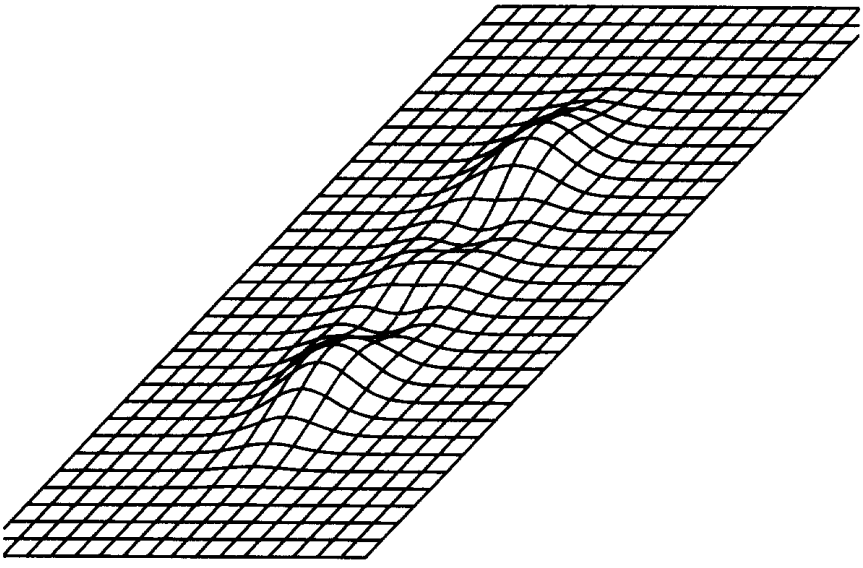

(*c*)

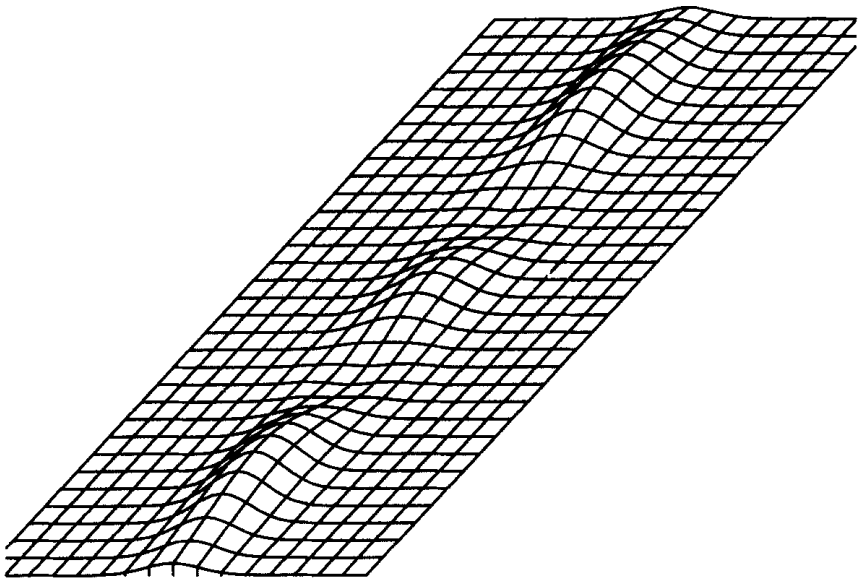

(*d*)

Figure 1. Dependence of the anti-normal quasi-distributions $\phi^2_{\mathscr{A}}(\alpha)$ for the state $|\beta=0, m=2\rangle_g$ on the squeeze parameter v. Cases (*a*)–(*d*) correspond to $v=0, 0{\cdot}5, 1, 2$.

would expect from the analogy with a squeezed vacuum. Dramatic changes follow when the two opposite boundaries of $\phi_{\mathscr{A}}$ touch themselves. That this moment arises can be anticipated from the fact that the opposite boundaries seem not to become thinner in the squeezing process. A transfer from an eliptic state towards a hill-like $\phi_{\mathscr{A}}$ follows. This can be seen in figures 1 (*b*) and (*c*). These hills in $\phi_{\mathscr{A}}$ further separate themselves and give rise to discontinuous $\phi_{\mathscr{A}}$ resulting in 'dashed-line' states (see [11]).

We will examine the described process by analysing (3.11). This is a product of three terms; a power term, a complex Hermite polynomial and the wall-like term $|\langle\alpha|\beta\rangle_g|^2$. Hermite polynomials have all zeros on the real axis, and as can be seen from (3.11) their argument is real (setting the condition $v>0$) on the imaginary axis of α. The zeros form local minima of the term $|H_m|$ in the complex plane α. For a very small $|v|$, they are all close to the point $\alpha=0$, as can be seen from the argument of H_m. At the same time, for usual α only the leading term is important in H_m. This term multiplied by the prefactor $|v/2\mu|^m$ then gives the power term in (3.12). As $|v|$ becomes larger, zeros of H_m move toward higher α, but the prefactor $|v/2\mu|^m$ suppresses the structured term $|H_m|$, and an interference of $|v/2\mu|^m$ and $|\langle\alpha|\beta\rangle_g|^2$ gives the eliptic $\phi_{\mathscr{A}}$. Only for a relatively large $|v|$ the term $|v/2\mu|^m$ grows up and $|H_m|$ appears. For such a large value of $|v|$ the strongly wall-like term $|\langle\alpha|\beta\rangle_g|^2$ suppresses all $|H_m|$ but the surrounding of the imaginary axis, where zeros are lying. As a result we see only hills, lying between the zeros (see figure 1 (*d*)).

$\phi^m_{\mathscr{A}}$ in (3.11) is formed by $\phi^0_{\mathscr{A}}$ multiplied by some polynomials. Since $\phi^0_{\mathscr{N}}$ does not exist, it is obvious that $\phi^n_{\mathscr{N}}$ does not exist for all m [8]. Note that the argument of the exponential function $|\langle\alpha|\beta\rangle_g|^2$ in (3.11) can be expressed in the form of a convariance matrix [8] or that shown in [14].

Let us consider photon-number distributions $p(n)$ for $|\beta, m\rangle_g$. $p(n)$ is equal to the square of the absolute value of the matrix element $\langle n|\beta, m\rangle_g$. This can be gained in the same way as $\langle\alpha|\beta, m\rangle_g$ (from the matrix elements $\langle n|\beta\rangle_g$). The analytical

expression for $\langle n|\beta,m\rangle_g$, found in the Appendix, reads

$$\langle n|\beta,m\rangle_g=\left(\frac{n!}{m!\mu}\right)^{1/2}\left(\frac{\nu}{2\mu}\right)^{n/2}\exp\left(-\frac{|\beta|^2}{2}+\frac{\nu^*}{2\mu}\beta^2\right)\sum_{i=0}^{\min(m,n)}\binom{m}{i}\frac{(2/\mu\nu)^{i/2}}{(n-i)!}$$
$$\times\left[\left(-\frac{\nu^*}{2\mu}\right)^{(m-i)/2}\right]H_{n-i}\left(\frac{\beta}{(2\mu\nu)^{1/2}}\right)H_{m-i}\left(\frac{-\alpha_0^*}{(-2\mu\nu^*)^{1/2}}\right), \tag{3.13}$$

and $p(n)$ finally results as

$$p(n)=|\langle n|\beta,m\rangle_g|^2. \tag{3.14}$$

Numerical examples for $p(n)$ and various parameters of the field $|\beta,m\rangle_g$ are described in section 6.

An interesting result are the wavefunctions $\langle q|\beta,m\rangle_g$. We can obtain them with the help of the completeness relation

$$\int|\alpha\rangle\langle\alpha|\frac{d^2\alpha}{\pi}=1, \tag{3.15}$$

the integral [15]

$$\int\exp\left[-B|\beta|^2+(C/2)\beta^{*2}+(C_1/2)\beta^2+D_1\beta+D\beta^*\right]d^2\beta$$
$$=\frac{\pi}{\sqrt{K}}\exp\left\{\frac{1}{K}\left[DD_1B+D^2(C_1/2)+D_1^2(C/2)\right]\right\}, \tag{3.16}$$
$$K=B^2-CC_1,\qquad \mathrm{Re}\,K>0,\qquad \mathrm{Re}\left[B+(C_1+C)/2\right]>0,$$

the generating function for Hermite polynomials [7] and (A 2). After a straightforward calculation $\langle q|\beta,m\rangle_g$ follows

$$\langle q|\beta,m\rangle_g=\frac{1}{\sqrt{m!}}\frac{\partial^m}{\partial\lambda^m}\int\langle q|\alpha\rangle\langle\alpha|S(\zeta)D(\beta)\exp(\lambda a^+)|0\rangle\frac{d^2\alpha}{\pi}\bigg|_{\lambda=0}$$
$$=\left(\frac{\omega}{\pi\hbar}\right)^{1/4}\frac{1}{((\mu-\nu)m!)^{1/2}}\exp\left\{\frac{1}{2}\left[-\frac{\mu+\nu}{\mu-\nu}(Q-Q_0)^2+\beta^2\frac{\mu^*+\nu^*}{\mu+\nu}-|\beta|^2\right]\right\}$$
$$\times(\sqrt{A})^mH_m\left(\frac{B}{2\sqrt{A}}\right), \tag{3.17}$$

where the coefficients are

$$Q=q\left(\frac{\omega}{\hbar}\right)^{1/2},\qquad Q_0=\frac{\beta\sqrt{2}}{\mu+\nu},\qquad A=\frac{1}{2}\frac{\mu^*-\nu^*}{\mu-\nu},\qquad B=\frac{Q\sqrt{2}}{\mu-\nu}+\frac{\nu}{\mu}(\beta^*-2A\beta).$$

In (3.17) we have used the element $\langle q|\alpha\rangle$ from [12]

$$\langle q|\alpha\rangle=\left(\frac{\omega}{\pi\hbar}\right)^{1/4}\exp\left(-\frac{Q^2}{2}+\alpha Q\sqrt{2}-\frac{1}{2}|\alpha|^2-\frac{1}{2}\alpha^2\right).$$

The wavefunctions $\langle p|\beta,m\rangle_g$ or $\langle\alpha_1|\beta,m\rangle_g$ (see [8]) can be deduced analogously.

The scalar product of $|\beta_1,m_1\rangle_g$ with $|\beta_2,m_2\rangle_g$, having different β_2, ζ_2, m_2, can be found similarly as $\langle q|\beta,m\rangle_g$. We simply replace $\langle q|\alpha\rangle$ by ${}_g\langle\beta_2,m_2|\alpha\rangle$ in (3.17) in its 'unwrapped' form (A 3) and use another coefficient λ' in place of λ. After the

integration in (3.17), differentiation after λ, λ' and a little algebra, the result acquires the form

$$
\begin{aligned}
{}_g\langle\beta_2, m_2|\beta_1, m_1\rangle_g = & \frac{1}{(\mu_1\mu_2 K m_1! m_2!)^{1/2}} \\
& \times \exp\left\{-\tfrac{1}{2}(|\beta_1|^2+|\beta_2|^2)+\frac{1}{\mu_1\mu_2^*-\nu_1\nu_2^*}\beta_2^*\beta_1\right. \\
& \left.-\frac{\nu_1\mu_2-\mu_1\nu_2}{2(\mu_1\mu_2^*-\nu_1\nu_2^*)}\beta_2^{*2}+\frac{(\nu_1\mu_2-\mu_1\nu_2)^*}{2(\mu_1\mu_2^*-\nu_1\nu_2^*)}\beta_1^2\right\} \\
& \times \sum_{j=0}^{m}\binom{m}{j}T^j(-A_1)^{(m'+j)/2}[(-\mathscr{A}_2)^{(m-j)/2}H_{m'+j} \\
& \times \left(\frac{B_1}{2(-A_1)^{1/2}}\right)H_{m-j}\left(\frac{B_2-B_1T}{2(-\mathscr{A}_2)^{1/2}}\right),
\end{aligned}
\tag{3.18}
$$

where the coefficients are

$$
\left.
\begin{aligned}
&A_1=\nu_1^*/2\mu_1-(\nu_2^*/2\mu_2^*)/K, \qquad A_2=\nu_2/2\mu_2^*-(\nu_1/2\mu_1)/K, \\
&B_1=-\alpha_{01}^*+[B_2^*/\mu_2^*-(2\beta_1/\mu_1)(\nu_2^*/2\mu_2^*)]/K, \\
&B_2=-\alpha_{02}+[\beta_1/\mu_1-(2\beta_2^*/\mu_2^*)(\nu_1/2\mu_1)]/K, \\
&K=1-\nu_1\nu_2^*/\mu_1\mu_2^*, \qquad T=1/2A_1K, \qquad \mathscr{A}_2=A_2-1/4A_1K^2
\end{aligned}
\right\}
\tag{3.19}
$$

To obtain (3.18) we transformed λ, λ' to other coefficients by the linear transformation ($\rho'=\lambda'$, $\rho=\lambda+T\lambda'$) since they appeared after integration in a common product. (3.18) agrees with the result from [8] for $m=m'=0$. To imagine the scalar product from (3.18), we can say that it arises from an interference of $\phi_{\mathscr{A}}^m$ with $\phi_{\mathscr{A}}^{m'}$, both of which can be differently squeezed and displaced in the plane α.

4. Degenerate parametric amplification with classical pumping of $D(\beta)|m\rangle$

In section 5 we describe damping of $|\beta, m\rangle_g$. For this task we have to find a one-parametric generating function of $\phi_{\mathscr{A}}^m(\alpha)$ for $|\beta, m\rangle_g$, we call this the 'unwrapped' form of $\phi_{\mathscr{A}}^m(\alpha)$. By this we mean $\phi_{\mathscr{A}}$ as a function of some parameter, which generates $\phi_{\mathscr{A}}^m(\alpha)$ for $m>0$; similarly as $\langle\alpha|S(\zeta)D(\beta)\exp(\lambda a^+)|0\rangle$ generates $\langle\alpha|\beta, m\rangle_g$ in (A 5). In principle we could use a two-parametric generating function of $\phi_{\mathscr{A}}^m(\alpha)$ in the form of the product of the matrix element $\langle\alpha|S(\zeta)D(\beta)\exp(\lambda a^+)|0\rangle$ with its complex conjugate, having the coefficient λ' in the place of λ in the same way as in (3.18). The differentiation after λ and λ' would give the correct $\phi_{\mathscr{A}}^m(\alpha)$, but if we make a number of transformations of the type (3.16) with such a two-parametric generating function it will soon become cumbersome for differentiation after λ, λ'. We will show how the one-parametric 'unwrapped' $\phi_{\mathscr{A}}^m(\alpha)$ can be deduced.

Consider the following quadratic Hamiltonian

$$
H=\hbar\omega(a^+a+\tfrac{1}{2})-\tfrac{1}{2}\hbar g[a^2\exp(2i\omega t-ie)+\text{H.c.}], \tag{4.1}
$$

where ω is the frequency, g the interaction constant and e the phase of the classical field. The evolution operator in the interaction picture of (4.1) acquires the form of

the squeezing operator (2.5). The solution of the Heisenberg equations for a and a^+ follows [14]

$$a(t)=u(t)a(0)+v(t)a^+(0), \qquad a^+(t)=[a(t)]^+, \tag{4.2}$$

where

$$u(t)=\exp(-i\omega t)\cosh(gt), \qquad v(t)=i\exp(-i\omega t+ie)\sinh(gt). \tag{4.3}$$

We will use the Heisenberg–Langevin approach [7] for performing the evolution of displaced Fock states $D(\beta)|m\rangle$ as the input of (4.1).

We observe in (3.12) that $\phi^m_{\mathscr{A}}(\alpha)$ for the states $D(\beta)|m\rangle$ can be found in the following way,

$$\phi^m_{\mathscr{A}}(\alpha)=\frac{(-1)^m}{\pi m!}\frac{\partial^m}{\partial\lambda_0^m}\exp(-\lambda_0|\alpha-\beta|^2)\Big|_{\lambda_0=1}. \tag{4.4a}$$

This leads us towards the 'unwrapped' one-parametric representation of $\phi^m_{\mathscr{A}}$ for displaced Fock states

$$\phi_{\mathscr{A}}(\alpha,\lambda_0)=\frac{1}{\pi}\exp(-\lambda_0|\alpha-\beta|^2). \tag{4.4b}$$

Squeezing it now in (4.1), results in the one-parametric $\phi_{\mathscr{A}}$ for $|\beta,m\rangle_g$.

Note that if we insert $\lambda_0=1/(\bar{n}+1)$ instead of $\lambda_0=1$ in (4.4a) and divide the expression by $(\bar{n}+1)^{m+1}$, where $\bar{n}$ is the number of chaotic photons, we obtain a generalization of $\phi^m_{\mathscr{A}}$ for a superposition of the state $D(\beta)|m\rangle$ with a chaotic field.

We will proceed in the following way [7]. First we find an anti-normal characteristic function $C_{\mathscr{A}}$, then a generating function $C^{(w)}_{\mathscr{N}}$, and finally photon-number distributions $p(n)$ and factorial moments $\langle W^k\rangle_{\mathscr{N}}$. The end of the present section is devoted to $\phi_{\mathscr{A}}$, needed in section 5.

Inserting (4.4b) and (4.2) into (3.2) and applying (A 1) to it to perform anti-normal re-ordering [7], we gain the one-parametric $C^m_{\mathscr{A}}$ for $|\beta,m\rangle_g$ in the 'unwrapped' form

$$C_{\mathscr{A}}(\xi,\xi^*,t)=\frac{1}{\pi}\int\exp(-\lambda_0|\alpha-\beta|^2+x+\alpha^*k-\alpha k^*)\,d^2\alpha=\frac{\exp(v)}{1-p}\exp\left(\frac{-pz}{1-p}\right), \tag{4.5}$$

$$x=-\tfrac{1}{2}(\xi^2uv+\text{c.c.})+|\xi|^2|v|^2, \quad y=x-z+\beta^*k-\beta k^*, \quad z=|k|^2, \quad k=\xi u^*-\xi^*v,$$

where (3.16) and the substitution $\lambda_0=1-p$ have been used. Thus the final form of $C^m_{\mathscr{A}}$, extending the differentiations from (4.4a) into (4.5) and employing the generating function for Laguerre polynomials [17], reads

$$C^m_{\mathscr{A}}(\xi,\xi^*,t)=\frac{1}{m!}\exp(y)\,L^0_m(z). \tag{4.6}$$

We can continue with the generating function $C^{(w)}_{\mathscr{N}}$. Making use of (3.6), (3.4), (3.16) and (4.5) the result follows

$$C^{(w)}_{\mathscr{N}}(\lambda)=\frac{1}{\lambda_0(1-\lambda/\lambda_1)(1-\lambda/\lambda_2)}\exp\left[\frac{\lambda\tau_1}{(1-\lambda/\lambda_1)}+\frac{\lambda\tau_2}{(1-\lambda/\lambda_2)}\right], \tag{4.7}$$

where the parameters are

$$\left.\begin{aligned} X&=(u^*v^*A^2+\text{c.c.})\left(\frac{1}{\lambda_0}-\frac{1}{2}\right)-\left[\frac{1}{\lambda_0}(|u|^2+|v|^2)-(1+|v|^2)\right]|A|^2,\\ Y&=1+|v|^2-\frac{1}{\lambda_0}(|u|^2+|v|^2), \qquad Z=|uv|^2\left(\frac{2}{\lambda_0}-1\right)^2, \qquad \lambda_{1,2}=\frac{1}{Y\pm\sqrt{Z}},\\ \tau_1&=\frac{\lambda_1 X-|A|^2}{1-\lambda_1/\lambda_2}, \qquad \tau_2=\frac{\lambda_2 X-|A|^2}{1-\lambda_2/\lambda_1}, \qquad A=-\beta u-\beta^* v. \end{aligned}\right\} \tag{4.8}$$

$C_{\mathcal{N}}^{(w)}$ from (4.7) generates the photon-number distributions $p(n)$ and the factorial moments $\langle W^k\rangle_{\mathcal{N}}$ in 'unwrapped' forms. Employing (3.7, 8) $p(n)$ results as in [14],

$$\begin{aligned} p(n)=&\frac{1}{\lambda_0}(EF)^{-1/2}(1-1/F)^n\exp(\tau_1/E+\tau_2/F)\sum_{i=0}^{n}\frac{1}{\Gamma(i+1/2)}\\ &\times\frac{1}{\Gamma(n-i+1/2)}\left(\frac{1-1/E}{1-1/F}\right)^i L_i^{-1/2}\left(\frac{\tau_1}{E(E-1)}\right)L_{n-i}^{-1/2}\left(\frac{\tau_2}{F(F-1)}\right), \end{aligned} \tag{4.9}$$

where $E=1-1/\lambda_1$, $F=1-1/\lambda_2$, Γ are Gamma functions and L_j^i are Laguerre polynomials [17]. The formulae (4.9), and (4.10) will be referred to in section 5 in connection with the damped $p(n)$ or $\langle W^k\rangle_{\mathcal{N}}$. Since we know $p(n)$ for $m>0$ from (3.14), we can go on with $\langle W^k\rangle_{\mathcal{N}}$,

$$\langle W^k\rangle_{\mathcal{N}}=\frac{1}{\lambda_0}k!(F-1)^k\sum_{i=0}^{k}\frac{1}{\Gamma(i+1/2)\Gamma(k-i+1/2)}\left(\frac{E-1}{F-1}\right)^i L_i^{-1/2}(-\lambda_1\tau_1)L_{k-i}^{-1/2}(-\lambda_2\tau_2). \tag{4.10}$$

For $m>0$ (4.10) must be differentiated as in (4.4a). The relation $\mathrm{d}L_n^i(x)/\mathrm{d}x=-L_{n-1}^{i+1}(x)$ [17] and the fact that $\lambda_{1,2}$ and $\tau_{1,2}$ are functions of λ_0 must be respected. Unfortunately, closed formulae do not exist even in the limiting cases $\beta=0$ or $v=0$, so that the procedure is rather different for every m.

We can close this section with the squeezed $\phi_{\mathcal{M}}(\alpha,t)$ for $C_{\mathcal{M}}$ from (4.5). Inserting (4.5) into (3.5) and using (3.16), $\phi_{\mathcal{M}}$ directly follows as

$$\phi_{\mathcal{M}}(\alpha,\alpha^*,t)=\frac{1}{\pi\lambda_0\sqrt{K_0}}\exp\left\{\frac{1}{K_0}[-B_0|A+\alpha|^2+(C^0/2)(A+\alpha)^{*2}+\text{c.c.}]\right\}, \tag{4.11}$$

where

$$B_0=1/\lambda_0(|u|^2+|v|^2)-|v|^2, \qquad C^0/2=uv(1/\lambda_0-1/2), \qquad K_0=B_0^2-|C^0|^2. \tag{4.12}$$

In (4.11) we dispose of the one-parametric $\phi_{\mathcal{M}}^m$ in the 'unwrapped' form. By changing $u\to\mu$, $v\to -v$ and $\lambda_0\to 1$, it approaches the correct limit of the square of the absolute value of (A 2). Here we will not use $\phi_{\mathcal{M}}$ from (4.11) to generate $\phi_{\mathcal{M}}^m$ for $m>0$, because they are known from (3.11), but the generating function $\phi_{\mathcal{M}}$ will be put as an input of a damping process in section 5.

5. Damping of the states $|\beta,m\rangle_\varrho$

Consider the Hamiltonian for a single-mode radiation interacting with a reservoir of phonon modes [7],

$$H=\hbar\omega a^+a+\sum_i\hbar(\omega_i b_i^+b_i+k_i b_i a^+ +k_i^* b_i^+ a), \tag{5.1}$$

where ω_i, and k_i are the frequency and interaction constant corresponding to the ith mode respectively. The generalized master equation in the Markoff approximation [12] and in the interaction picture for (5.1) reads

$$\frac{\partial\rho}{\partial t}=\frac{\gamma}{2}(2a\rho a^+-a^+a\rho-\rho a^+a)+\gamma\bar{n}(a^+\rho a+a\rho a^+-a^+a\rho-\rho aa^+), \tag{5.2}$$

where γ is the damping rate and $\bar{n}$ the mean number of chaotic phonons.

$\phi_{\mathscr{A}}$ for the damping process described by (5.2) can be found by the standard method of the Green function for the Fokker–Planck equation of (5.2). The Fourier transform of this $\phi_{\mathscr{A}}$ gives the damped $C_{\mathscr{A}}$ [12],

$$C_{\mathscr{A}}(\alpha,\alpha^*,t)=\int\phi_{\mathscr{A}}(\alpha,\alpha^*)\exp[-|\xi|^2\zeta'+(\xi\alpha^*-\xi^*\alpha)\exp(-\gamma t/2)]\,\mathrm{d}^2\alpha, \tag{5.4}$$

$$\zeta'=(\bar{n}+1)[(1-\exp(-\gamma t)], \tag{5.5}$$

which is directly related to $\phi_{\mathscr{A}}(\alpha,\alpha^*)$ at the input.

We will proceed in the same way as for section 4, inserting the one-parametric $\phi_{\mathscr{A}}$ from (4.11) into (5.4) and using (3.16) as before. The 'unwrapped' one-parametric $C_{\mathscr{A}}$ for damped $|\beta,m\rangle_g$ follows

$$\begin{aligned}C_{\mathscr{A}}(\alpha,\alpha^*,t)=\frac{1}{\lambda_0}\exp\{&\mathscr{D}-|\xi|^2[\zeta'+B_0\exp(-\gamma t)]+B_0\exp(-\gamma t/2)(d^*\xi-d\xi^*)\\&+(C^0/2)^*[2d\xi\exp(-\gamma t/2)+\xi^2\exp(-\gamma t)]\\&+(C^0/2)[-2d^*\xi^*\exp(-\gamma t/2)+\xi^{*2}\exp(-\gamma t)]\},\end{aligned} \tag{5.6}$$

where the new parameters are

$$\begin{aligned}d&=-(B_0A+C^0A_1)/K_0,\\ \mathscr{D}&=B_0(|A|^2/K_0+|d|^2)+[(C^0/2)^*(A^2/K_0+d^2)+\text{c.c.}].\end{aligned} \tag{5.7}$$

The structure of (5.6) is $\exp[L_1(\lambda_0)/L_2(\lambda_0)]/\lambda_0$, where $L_i(\lambda_0)$ are polynomials of a fourth degree. This is the form of (4.7) with four fractions in the exponent. Unfortunately, closed formula for $m>0$ from this generating function cannot be obtained, even by a numerical computation of the roots in the fractions (see the first paper in [2]), because $C^m_{\mathscr{A}}$ must be differentiated at the end after ξ and ξ^*.

We have found $C^m_{\mathscr{A}}$ in the two limit cases (*a*) $\beta=0$, (*b*) $v=0$, for which $\mathscr{D}=0$. After simple algebra $C_{\mathscr{A}}$ and $C^m_{\mathscr{A}}$ for these cases can be rearranged in the forms (4.5) or (4.6) with the coefficients (x, z in (*a*) are from (4.5))

$$(a)\quad y_a=(x-z)\exp(-\gamma t)-\zeta'|\xi|^2,\qquad z_a=z\exp(-\gamma t), \tag{5.8a}$$

$$(b)\quad y_b=-|\xi|^2(\zeta'+\exp(-\gamma t))+\exp(-\gamma t/2)(\beta^*\xi-\beta\xi^*),\qquad z_b=|\xi|^2\exp(-\gamma t). \tag{5.8b}$$

Let us search out several damped moments, making use of (3.9) and

$$\begin{aligned}\left\langle\left(\Delta\begin{matrix}q\\p\end{matrix}\right)^2\right\rangle&=1\pm[\langle(\Delta a)^2\rangle+\langle(\Delta a^+)^2\rangle]+2\langle\Delta a^+\Delta a\rangle\\&=1\pm[\langle a^{+2}\rangle+\langle a^2\rangle-\langle a^+\rangle^2-\langle a\rangle^2]+2(\langle a^+a\rangle-\langle a^+\rangle\langle a\rangle),\end{aligned} \tag{5.9}$$

we obtain for the two limits

$$\left.\begin{aligned}
&(a)\quad \langle a\rangle = 0,\\
&\langle a^2\rangle = \frac{1}{m!}\exp(-\gamma t)uv[L_m^0(0)+2L_{m-1}^1(0)],\\
&\langle aa^+\rangle = \frac{1}{m!}[(\zeta'+\exp(-\gamma t)|u|^2)L_m^0(0)+L_{m-1}^1(0)(|u|^2+|v|^2)\exp(-\gamma t)],\\
&\left\langle\left(\Delta\begin{matrix}q\\p\end{matrix}\right)^2\right\rangle = 1\pm\frac{1}{m!}\exp(-\gamma t)[L_m^0(0)+2L_{m-1}^1(0)](uv+u^*v^*)+2(\langle aa^+\rangle-1),
\end{aligned}\right\}\quad(5.10a)$$

$$\left.\begin{aligned}
&(b)\quad \langle a\rangle = \frac{1}{m!}[\beta\exp(-\gamma t/2)\,L_m^0(0)],\\
&\langle a^2\rangle = \frac{1}{m!}[\beta^2\exp(-\gamma t)\,L_m^0(0)],\\
&\langle aa^+\rangle = \frac{1}{m!}\{[\zeta'+\exp(-\gamma t)]\,L_m^0(0)+\exp(-\gamma t)\,[|\beta|^2L_m^0(0)+L_{m-1}^1(0)]\},
\end{aligned}\right\}\quad(5.10b)$$

where $L_m^k(0)=[(m+k)!]^2/(m!k!)$. In (5.10) we employed the relation $\langle aa^+\rangle = 1+\langle a^+a\rangle$, holding in the Schrödinger–Markoff picture, where commutation relations are preserved [12]. Further moments will be deduced by the Heisenberg–Langevin method in section 6 and presented by numerical examples.

We can concentrate on the damped generating function $C_{\mathcal{N}}^{(w)}$. By inserting $C_{\mathcal{A}}$ from (5.6) into (3.4, 6) and suitably rearranging the result, we obtain $C_{\mathcal{N}}^{(w)}$ in the form (4.7) multiplied by $\exp\{\mathcal{D}\}$. The photon-number distributions $p(n)$, and factorial moments $\langle W^k\rangle_{\mathcal{N}}$ derived from it, acquire the forms, shown in (4.9) and (4.10), both multiplied by $\exp\{\mathcal{D}\}$. The new coefficients follow

$$\left.\begin{aligned}
&X = -[\zeta'+B_0\exp(-\gamma t)-1]|\sigma|^2+[(\rho/2)^*\sigma^2+\text{c.c.}],\\
&Y = 1-[\zeta'+B_0\exp(-\gamma t)],\\
&Z = |C^0|^2\exp(-2\gamma t), \qquad \rho/2 = (C^0/2)\exp(-\gamma t),\\
&\sigma = -\exp(-\gamma t/2)\,(B_0d+C^0d^*),
\end{aligned}\right\}\quad(5.11)$$

where $\lambda_1, \lambda_2, \tau_1, \tau_2$ have the same structure as in (4.8), changing the term $|A|^2$ by $|\sigma|^2$ in the explicit forms of τ_1 and τ_2. Rearranging of $p(n)$ and $\langle W^k\rangle_{\mathcal{N}}$ for $m>0$, after the differentiation under λ_0, is governed by the same barriers as in (4.10). Therefore we present a numerical approach to $p(n)$ in section 6.

Finally, it remains to find the one-parametric damped $\phi_{\mathcal{A}}$ for $C_{\mathcal{A}}$ from (5.6). We use (3.5) and find out that $\phi_{\mathcal{A}}$ acquires the form of the result of the integral in (3.16), multiplied by the factor $\exp\{\mathcal{D}\}/\pi^2\lambda_0$. The coefficients are, after the replacement of C and C_1 in (3.16) by ρ and ρ^*,

$$B = \zeta'+B_0\exp(-\gamma t), \qquad D = \sigma+\alpha, \qquad D_1 = -D^*. \tag{5.12}$$

As regards rearranging of $\phi_{\mathcal{A}}$ for $m>0$, the situation is the same as with $C_{\mathcal{A}}$ in (5.6), but now polynomials of the sixth degree should be used. Since $\phi_{\mathcal{A}}^m$ need not be differentiate in contrast with $C_{\mathcal{A}}^m$, this enables us to obtain a closed formula for $\phi_{\mathcal{A}}^m$, when numerically computing the sixth roots and differentiating such a generating

function. We do not attempt this procedure and consider $\phi_{\mathscr{A}}$ in the above limits (5.8). Results appear very simply.

Performing the differentiation from (4.4 *a*) onto $\phi_{\mathscr{A}}$ for the case (*a*), $\phi^m_{\mathscr{A}}$ acquires the form of (4.9), where the prefactor $1/\lambda_0$ is replaced by $1/(\pi\delta_0)$. The new coefficients are

$$\left.\begin{aligned}
&\delta_0=(|u|^2-|v|^2)^2\exp(-2\gamma t), \qquad \delta_2=[\zeta'-|v|^2\exp(-\gamma t)]^2-|uv|^2\exp(-2\gamma t),\\
&\delta_1=2(|u|^2+|v|^2)[\zeta'-|v|^2\exp(-\gamma t)]\exp(-\gamma t)+4|uv|^2\exp(-2\gamma t),\\
&\gamma_1=-(|u|^2+|v|^2)|\alpha|^2\exp(-\gamma t)+(\alpha^2u^*v^*+\text{c.c.})\exp(-\gamma t),\\
&\gamma_2=[|v|^2\exp(-\gamma t)-\zeta']|\alpha|^2-\tfrac{1}{2}(\alpha^2u^*v^*+\text{c.c.})\exp(-\gamma t),\\
&\tau_1=\frac{1}{\delta_0}\frac{\lambda_1\gamma_2+\gamma_1}{1-\lambda_1/\lambda_2}, \qquad \tau_2=\frac{1}{\delta_0}\frac{\lambda_2\gamma_2+\gamma_1}{1-\lambda_2/\lambda_1},\\
&\lambda_{1,2}=[-\delta_1+(\delta_1^2-4\delta_2\delta_0)^{1/2}]/(2\delta_2).
\end{aligned}\right\} \tag{5.13}$$

Examples for $m=1$, $gt=0, 0{\cdot}8, 1{\cdot}6$ and 3 and $\bar{n}=1$ are demonstrated in figure 2. We can see that damping leads to two effects appearing in $\phi^m_{\mathscr{A}}$. At first it produces, from the disconnected wall-like $\phi^m_{\mathscr{A}}$, a series of disconnected hills which move toward the coordinate centre (figure 2 (*b*)). Secondly, it smooths these hills in such a way that they start to produce continuous $\phi^m_{\mathscr{A}}$ (figure 2 (*c*)). For longer periods $\phi^m_{\mathscr{A}}$ approaches, as we would expect, a Gaussian form for a chaotic light with $\bar{n}=1$ chaotic photons.

Similarly $\phi^m_{\mathscr{A}}$ can be converted for (*b*). It acquires the form

$$\phi^m_{\mathscr{A}}(\alpha,\alpha^*,t)=\frac{\exp(+\gamma t)}{m!(1-\lambda_1)^{m+1}}\exp\left(\frac{\lambda_1 C}{\lambda_1-1}\right)L^0_m\left[\frac{-\lambda_1^2 C}{\lambda_1-1}\right], \tag{5.14}$$

where

$$C=-|\beta\exp(-\gamma t/2)-\alpha|^2\exp(+\gamma t), \qquad \lambda_1=-\frac{1}{\zeta'}\exp(-\gamma t). \tag{5.15}$$

We will look at the evolution of this damped $\phi^m_{\mathscr{A}}$ in more detail. It can be seen that first the ring of $\phi^m_{\mathscr{A}}$ (for small $\bar{n}$ and $|\beta|>m$) starts to move from the point $\alpha=\beta$ towards the centre of the coordinate system (as in the usual damping of a coherent state [7]). After a time of order $1/\gamma$ the ring diminishes and $\phi_{\mathscr{A}}$ for a coherent state develop in the moving centre of the original ring. For longer periods the process follows the damping of the coherent state. For greater $\bar{n}$ or $|\beta|<m$ an evolution is more blurred.

6. Numerical results and discussions

Although the above derived formulae are exact, in practice they could lead to considerable trouble. We will demonstrate how photon-number distributions and moments can be calculated numerically. Our interest concerns the states $|\beta,m\rangle_g$; (i) undamped, (ii) damped by one-photon, (iii) two-photon absorption.

6.1. *Undamped*

Numerical results for photon-number distributions $p(n)$ of the states $|\beta,m\rangle_g$ could be obtained from the expression (3.13) or can be found numerically in the form of a sum of scalar products of vectors $b^{+i}|n\rangle$ (b^+ from (2.9)) with $S(\zeta)D(\beta)|0\rangle$. We

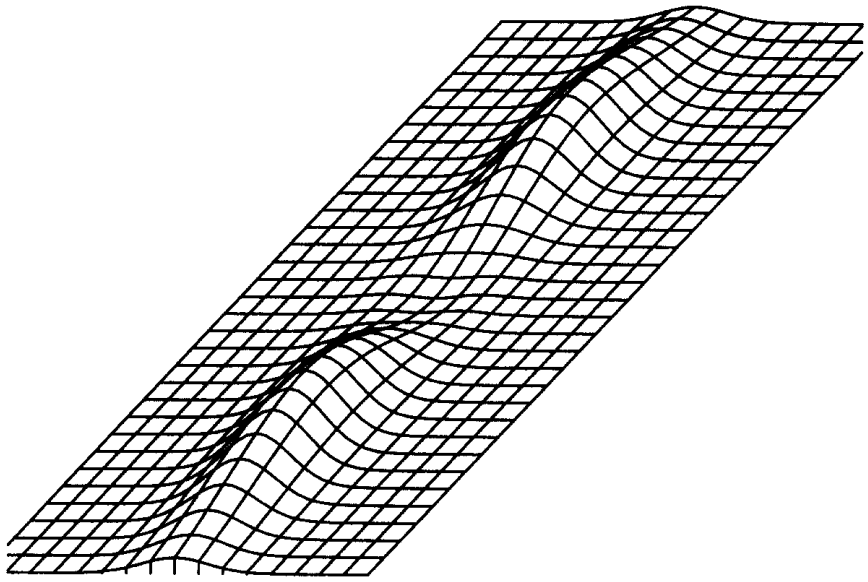

(*a*)

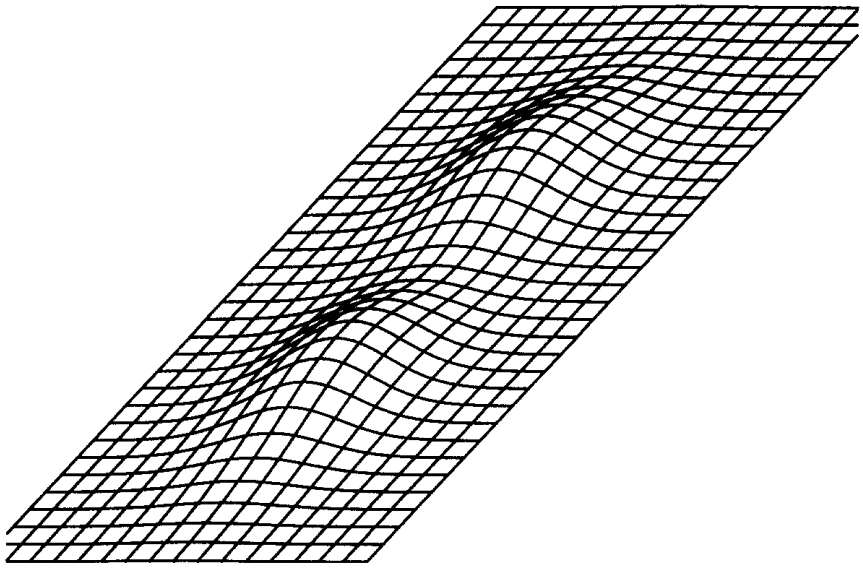

(*b*)

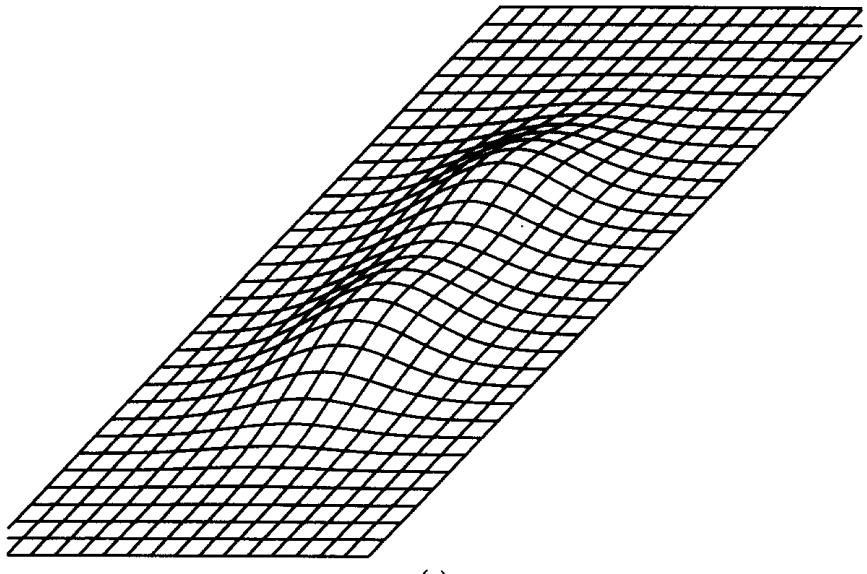

(*c*)

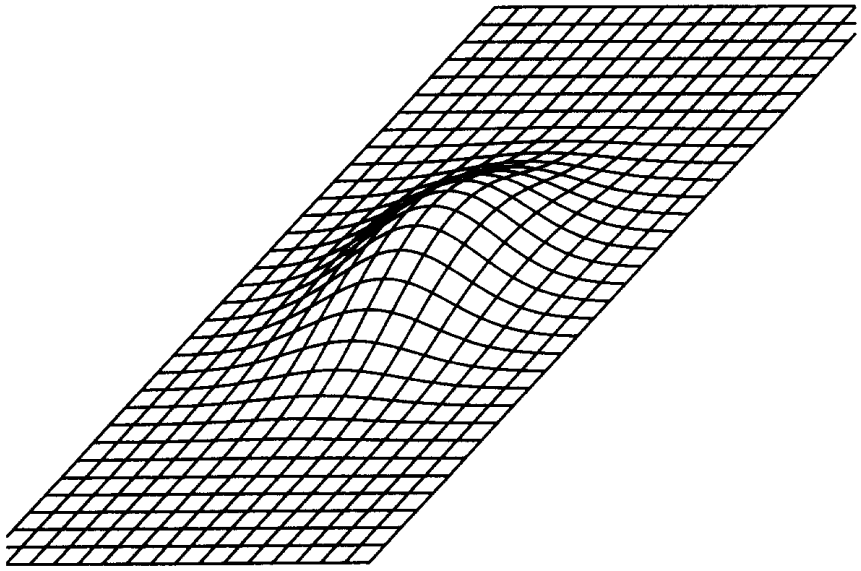

(*d*)

Figure 2. Time evolution of the damped anti-normal quasi-distributions $\phi^1_{\mathscr{A}}(\alpha)$ for the state $|\beta=0,\ m=1\rangle_g$ and $\nu=2$. Cases (*a*)–(*d*) correspond to $gt=0, 0{\cdot}8, 1{\cdot}6, 3$ and $\bar{n}=1$.

will clarify the last possibility. Employing the elements (A 7) and rules (2.8, 9) we get

$$\begin{aligned}\langle n|S(\zeta)D(\beta)|m\rangle &= \langle n|S(\zeta)D(\beta)\frac{a^{+m}}{\sqrt{m!}}|0\rangle \\ &= \frac{1}{\sqrt{m!}}\langle n|S(\zeta)(a^+-\beta^*)^m D(\beta)|0\rangle \\ &= \frac{1}{\sqrt{m!}}\langle n|(b^+-\beta^*)^m S(\zeta)D(\beta)|0\rangle \\ &= \frac{1}{\sqrt{m!}}\sum_{i=0}^{m}\binom{m}{i}(-\beta^*)^{m-i}\langle n|b^{+i}S(\zeta)D(\beta)|0\rangle. \end{aligned} \tag{6.1}$$

The term $b^{+i}=(\mu^* a^+ + \nu^* a)^i$ acts on $\langle n|$ as

$$\langle n|b^{+i}=[\langle n-1|\mu^*\sqrt{n}+\langle n+1|\nu^*(n+1)^{1/2}(\mu^* a^+ + \nu^* a)^{i-1}=\ldots . \tag{6.2}$$

This calculation and a final sum of elements $\langle k|S(\zeta)D(\beta)|0\rangle$ can be performed by computer. Some typical examples of $p(n)$ are demonstrated in figures 3–11.

Figures 3 and 4 pertain to shifted Fock states $D(\beta)|m\rangle$, for which it holds that [18]

$$p(n)=\frac{n!}{m!}\exp(-|\beta|^2)\,|\beta|^{2(m-n)}[L_m^{m-n}(|\beta|^2)]^2. \tag{6.3}$$

Figure 3 in particular shows $p(n)$ for the first four Fock states with $|\beta|=5$ ($\beta=\alpha_0$ for $\nu=0$). $\phi_{\mathscr{A}}$ for $|m\rangle$, displayed in (3.12), reaches a maximum at $|\beta|=\sqrt{m}$. These maxima are for $D(5)|3\rangle$ displaced to $|\alpha|^2=(5\pm\sqrt{3})^2$, which correspond approximately to the maxima of boundary peaks of $p(n)$, when $n=|\alpha|^2$ is substituted. For the chosen conditions the centre of the coordinate system lies outside the ring-like $\phi_{\mathscr{A}}$.

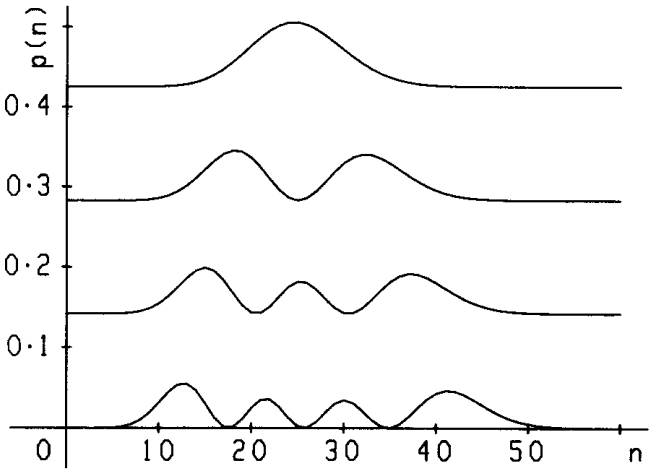

Figure 3. Photon number distribution $p(n)$ for the first four Fock states $|m=0\text{–}3\rangle$, displaced into the point $\alpha_0=5$. Ordering of the curves $m=0\text{–}3$ is from the top to the bottom.

In figure 4 we can see $p(n)$ for $D(\beta)|20\rangle$ with $\beta=0-1$ and the step 0·2. For $\beta=1$ the centre of the coordinate system lies inside the ring-like $\phi_{\mathscr{A}}$ and the maxima of $p(n)$ are approximately at $n=[(20)^{1/2}\pm 1]^2$. All curves pertain to the first region of sub-Poissonian behaviour described at the end of section 2.

Figure 5 demonstrates an evolution of $p(n)$ for $m=0\text{–}2$, $v=0\text{–}5$ and $\alpha_0=5$. For $v\neq 0$ we must take into account the angle of $\alpha_0=|\alpha_0|\exp(i\varphi)$ or μ, v. For $v\neq 0$ and $\mu=(1+v^2)^{1/2}$ from (2.7) we obtain $\phi_{\mathscr{A}}$ squeezed from the sides and its centre displaced into the point α_0 in the complex plane α. For $\varphi=0$ typical *fast* oscillations appear in $p(n)$. They arise by the interference of cigar-like $\phi_{\mathscr{A}}$ and the photon-number rings ($|\alpha|^2=$ integer). Thorough discussion of this phenomenon for $|\beta,0\rangle_g$ can be found in [13]. From (3.11) and figure 1 we expect *slow* oscillations when the photon-number

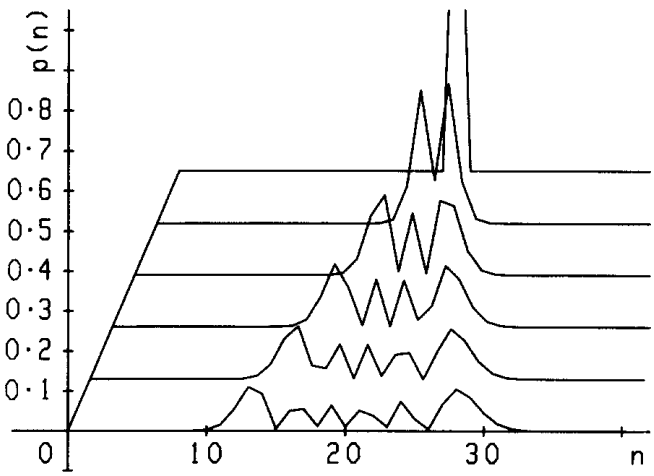

Figure 4. Dependence of the photon-number distribution $p(n)$ for the displaced twentieth Fock state $D(\alpha_0)|20\rangle$ on the displacing parameter α_0. Curves are ordered from behind with the parameter $\alpha_0=0, 0{\cdot}2, 0{\cdot}4, 0{\cdot}6, 0{\cdot}8, 1$.

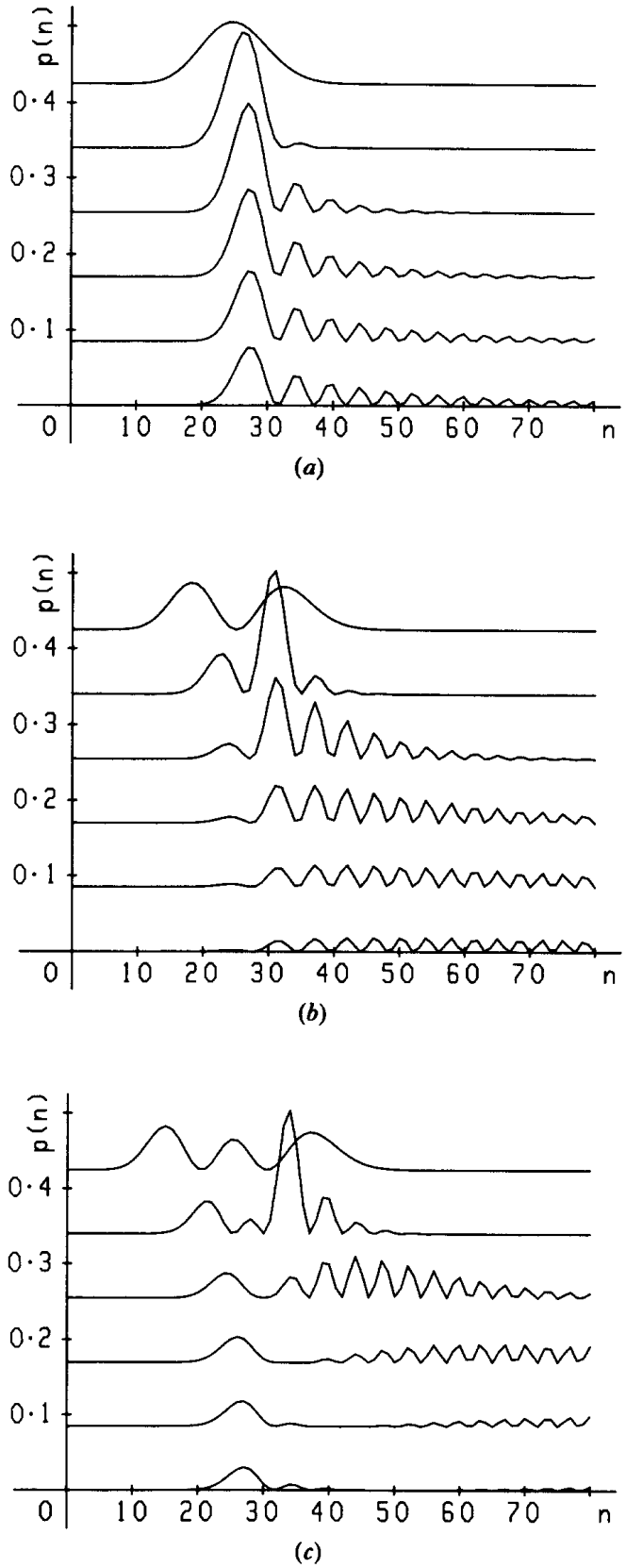

Figure 5. Dependence of the photon-number distribution $p(n)$ for the state $|\beta, m=0\text{–}2\rangle_g$ with $\alpha_0=5$ (connection between α_0 and β, μ, ν is in (2·4)) on ν, which varies as $\nu=0,1,2,3,4,5$ (growth of ν is from behind). Cases (*a–c*) correspond to $m=0\text{–}2$.

circles pass through the holes in $\phi_{\mathscr{A}}$. For $m=2$ and $\alpha_0=0$ we easily find the minima of $\phi^2_{\mathscr{A}}$ at $|\alpha_{\min}|^2=v(1+v^2)^{1/2}$. So that for $\alpha_0\neq 0$ and $\varphi=0$ the minimum in $p(n)$ should appear at the point $n=|\alpha_0|^2+|\alpha_{\min}|^2=|\alpha_0|^2+(1+v^2)^{1/2}$. For $v=3,4,5$ and $\alpha_0=5$ we have $n=34{\cdot}5, 41{\cdot}5, 50{\cdot}5$, which is in agreement with figure 5 (*c*). This figure represents an interference of the two holes in $\phi^2_{\mathscr{A}}$ with the photon-number circles. Similar falling of the photon-number distribution should arise for higher m at every hole pair, and when $\phi^m_{\mathscr{A}}$ rotates in the plane α at general hole pairs. The behaviour of peaks, having their centres at the smallest n in figures 5 (*a*)–(*c*), reflects an interference of the photon-number rings with the centre of $\phi_{\mathscr{A}}$. For odd m $\phi_{\mathscr{A}}$ has a central peak, for even m it does not. This results in jump-like or continuous behaviour of $p(n)$ for the smallest n. If the initial value of $p(n)$ for the smallest n is taken to indicate the fall of pressure in a whistle, for even m the whistle should be closed, for odd m it is opened. The number m then represents the exicted mode, and in $p(n)$ this is displayed by $(m+1)/2$ local maxima in slow oscillating peaks.

For $\varphi=\pi/2$ typical *two-photon* oscillations come out in $p(n)$. They arise whenever $|\alpha_0|$ is so small that $\phi_{\mathscr{A}}$ reaches the centre of the coordinate system and parts of $\phi_{\mathscr{A}}$ are on both its sides. Then the photon-number rings interfere with these parts, which results in oscillations. An example for $|\beta,1\rangle_g$, $\alpha_0=7\exp(\mathrm{i}\pi/2)$ and $v=1$–5 is shown in figure 6 (*a*). It is easy to deduce the maxima of $\phi_{\mathscr{A}}$ for $\varphi=\pi/2$. For $\phi^1_{\mathscr{A}}$ and $\alpha_0=0$ they are at $|\alpha|^2=1/(1-v/\mu)$, so that for $\alpha_0\neq 0$ they shift into $|\alpha'|^2=[|\alpha_0|+1/(1-v/\mu)^{1/2}]^2$. This approximately agrees with the maxima in $p(n)$, but it is not so simple to obtain the end of the two-photon oscillations. For $v=4$ the maxima of $\phi^1_{\mathscr{A}}$ are at $(7\pm 5,8)^2$, so that a long tail lies behind the coordinate centre and gives rise to them. It is convenient at this point to call attention to an interesting fact, that when $\phi_{\mathscr{A}}$ for $\varphi=\pi/2$ is sufficiently far from the coordinate centre, only slow oscillations (the same as in figure 3) appear in $p(n)$. In such a situation no new oscillations occur owing to the squeezing and the presence of holes in $\phi_{\mathscr{A}}$, only the oscillations from clearly displaced Fock states appearing in figure 3 are elongated to higher n, regardless of the fact that the structure of $\phi_{\mathscr{A}}$ dramatically changes. Figure 6 (*b*) shows the same as figure 6 (*a*) but for $\varphi=1,18$. All oscillations are now present and their eventual sources can hardly be separated. A consequence of $\varphi\neq 0$ is a transfer from a two-photon towards more slow, but less regular, oscillations, characteristic of figure 5.

In figure 7 $p(n)$ is demonstrated for rotating $\phi_{\mathscr{A}}$. The parameters are $m=2$, $\alpha_0=7\exp(\mathrm{i}\varphi)$, $v=2$ and φ varies from 0 to $\pi/2$, beginning at the lower curve. We can see a transition of $p(n)$ for a vertical $\phi_{\mathscr{A}}$, with its *two* main maxima (one of which is oscillating as in figure 5 (*c*)), appearing owing to the presence of holes in $\phi_{\mathscr{A}}$, towards $p(n)$ for a horizontal $\phi_{\mathscr{A}}$ with its *three* maxima (the first of which is brought by two-photon oscillations in analogy with figure 6 (*a*)).

In figure 8 we show $p(n)$ for $|0,20\rangle_g$ and $v=0$–$0,5$. If we consider the maximum and minimum boundary distances of the ring-elliptic $\phi^{20}_{\mathscr{A}}$ from the coordinate centre to be at $|\alpha|^2=20\,|\mu\pm v|^2$, we find the end positions of the row of peaks in a good agreement with figure 8. For $v=0{\cdot}3$ and $0{\cdot}4$ the boundaries are at $n=11{\cdot}1, 36{\cdot}1$, or $n=9{\cdot}2, 43{\cdot}6$ respectively. The structure of peaks gives the impression of bunching. For a small v the field $|\beta,m\rangle_g$ is sub-Poissonian, as in figure 4.

Figure 9 displays an evolution of $p(n)$ for $\alpha_0=0$–1 and the step $0{\cdot}2$, for the second curve $v=0{\cdot}1$ from figure 8. It can be observed that the central peak at $n=20$, which disappeared in figure 8, reappears and moves toward higher n. It corresponds to the most distant boundary of the squeezed elliptic $\phi^{20}_{\mathscr{A}}$, which interfers with photon-number rings. Similarly the hill-like peak corresponds to the nearest boundary. As

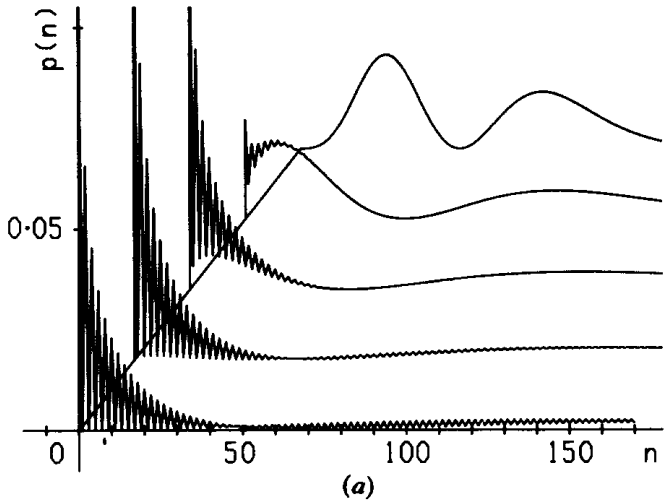

(*a*)

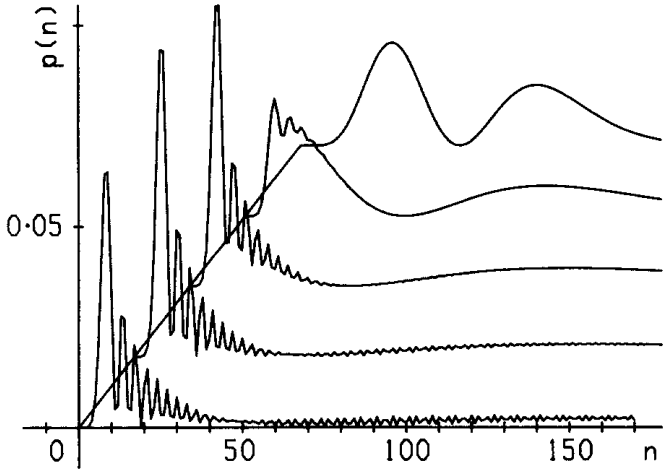

(*b*)

Figure 6. The same as in figure 5 for $|\beta, m=1\rangle_g$ and $\alpha_0=7\exp(i\varphi)$. The squeezing parameter v varies as $v=1,2,3,4,5$, starting from the back curve. The values of φ are $\varphi=\pi/2$, and $\varphi=1{\cdot}18$ for (*a*) and (*b*) respectively.

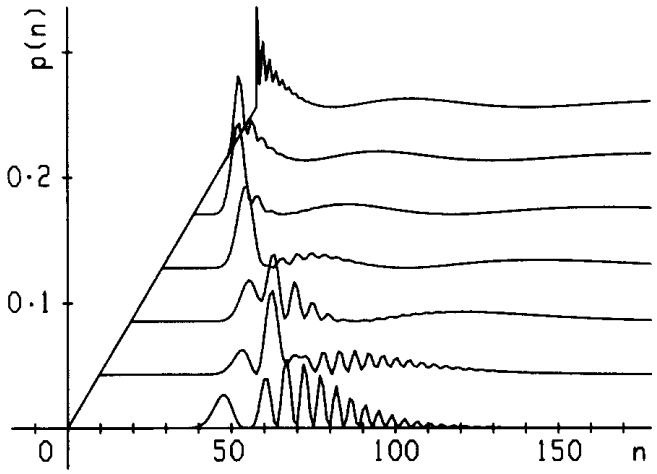

Figure 7. Dependence of the photon-number distribution $p(n)$ for the state $|\beta, m=2\rangle_g$ with $m=2$, $v=2$, $\alpha_0=7\exp(i\varphi)$ on the angle φ. Curves are ordered from behind with $\varphi=\pi/2$–0 and step $\pi/12$.

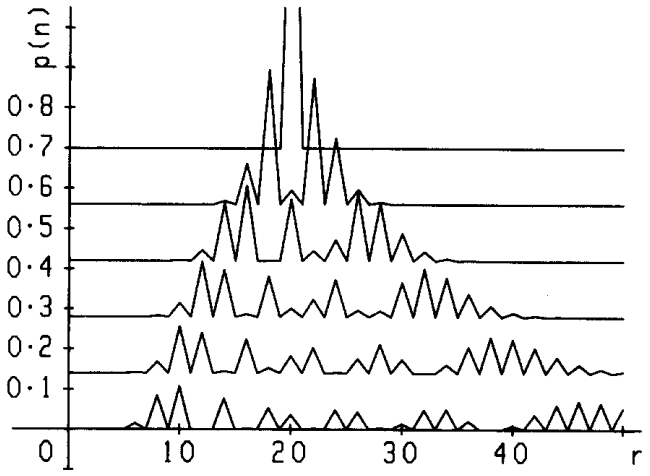

Figure 8. As figure 5, but for $|\beta, m=20\rangle_g$ with $\alpha_0=0$ and v varies from the top to the bottom with $v=0, 0{\cdot}1, 0{\cdot}2, 0{\cdot}3, 0{\cdot}4, 0{\cdot}5$.

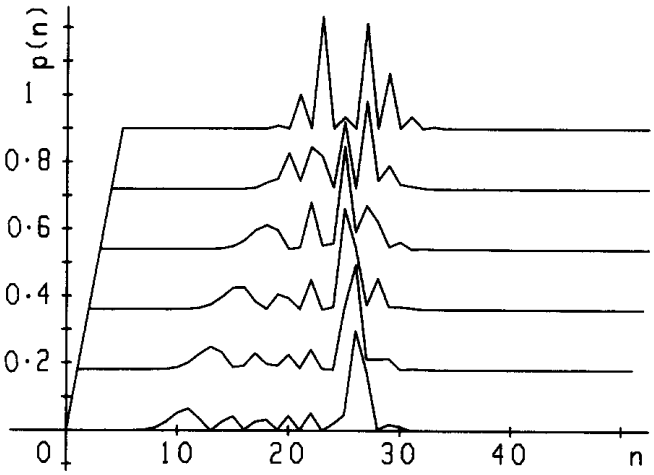

Figure 9. Dependence of the second curve from figure 8 for $v=0{\cdot}1$ on the parameter α_0. Curves are ordered from behind with $\alpha_0=0, 0{\cdot}2, 0{\cdot}4, 0{\cdot}6, 0{\cdot}8, 1$.

ϕ_{sd}^{20} is squeezed from the sides, the maximum and minimum boundary is approximately at $|\alpha|^2=|(20)^{1/2}|\mu\pm v|+\alpha_0|^2$. This agrees well with figure 9, where for $\alpha_0=0{\cdot}8$, or 1, we have $n=10{\cdot}5, 23{\cdot}5$, or $n=9{\cdot}3, 25{\cdot}5$ respectively.

Figures 10 (*a*) and (*b*) represent photon-number statistics for a displaced and squeezed chaotic density matrix (Bose–Einstein distribution) computed as a superposition of $p(n)$ for Fock states. The parameters are $n=0$–2 chaotic photons in the field, $\alpha_0=5$, $v=3$ and $\varphi=0$ and $\pi/2$. It is obvious from the statistics that chaotic photons smooth all oscillations. $p(n)$ for a superposition of $|\beta, m\rangle_g$ with $m>0$ and a chaotic field can be computed by the method described under the expression (4.4 *b*) and for $m=3$ it is presented in figure 12.

Note that an analysis of non-classical fields with non-zero noise has appeared in reference [19]. There investigation was performed starting from a Gaussian–Wigner function ϕ_s (see (3.5)) of a general form. ϕ_s functions employed there cover up those

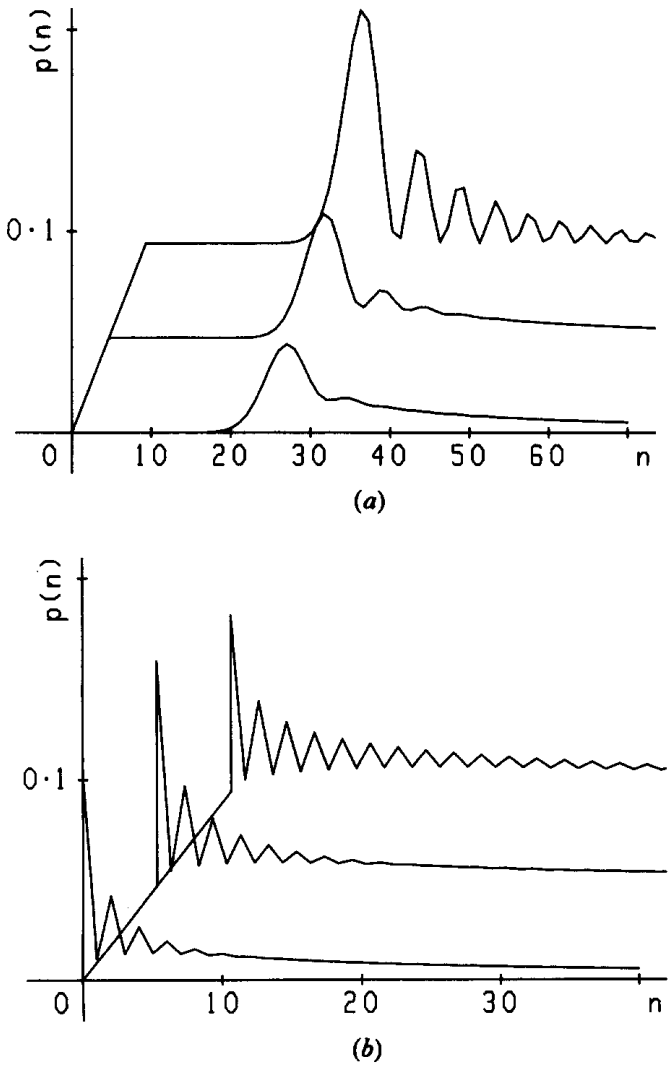

Figure 10. Dependence of the photon-number distributions $p(n)$ for a displaced and squeezed chaotic density matrix ρ with the parameters $\alpha_0 = 5\exp(i\varphi)$, $v = 3$ on the number of chaotic photons $\bar{n}$. (*a*) and (*b*) correspond to $\varphi = 0$ and $\varphi = \pi/2$ and the curves are ordered from behind with $\bar{n} = 0, 1, 2$.

ϕ_s which could be found by using (3.4) and (3.5) from $\phi_{\alpha\beta}$ with the parameters (5.12) and $m = 0$. For this case ϕ_s is really found in [19]. For $m > 0$ a more general class of functions should be chosen to describe a corresponding ϕ_s. This is clear from the fact that the $\phi_{\alpha\beta}$ for $m > 0$, found here, arises from those for $m = 0$ by a differentiation resulting in a pre-exponential polynomial. Analysis very similar to the present work appeared parallely in [20] where $|\beta, m\rangle_g$ states were investigated and their Wigner function ϕ_s, described above, were found. Both works deal with squeezed thermal states particularly, whose photon-number distributions are displayed in figure 10.

As regards the work done in [20] and the subsequent paper in *Phys. Rev.* from the same authors, quantum fluctuations, photon-number distributions and further interesting results, for squeezed thermal and Fock states, can be found there. In going beyond the scope of this paper it covers, for example, a generalized version of

ideas from [13], concerning an interpretation of oscillations in $p(n)$, resulting from interferences in a phase space.

Figure 11 (*a*) presents the reduced factorial moments $\langle(\Delta W)^2\rangle_{\mathcal{N}}/\langle W\rangle^2_{\mathcal{N}} = \langle W^2\rangle_{\mathcal{N}}/\langle W\rangle^2_{\mathcal{N}} - 1 = g^{(2)} - 1$, where $g^{(2)}$ is a second-order correlation function [7], for $|\beta, m\rangle_g$ found from (2.15) and (2.16) for $m = 0$–$3, 10\,500$, $\alpha_0 = 7$, $v = 0$–32. The curves are ordered from the lower $m = 0$ to the upper $m = 500$ at the point $v = 4$. Figure 11 (*b*) shows a detail of the sub-Poissonian behaviour of $|\beta, m\rangle_g$ with $m = 0, 1$ from figure 11 (*a*). These examples fall in the second region described at the end of the section 2.

6.2. *One-photon damping*

For investigation of damping of the states $|\beta, m\rangle_g$ it is more convenient to start from the generalized master equation (5.2). Acting on both its sides $\langle n|$ and $|n\rangle$

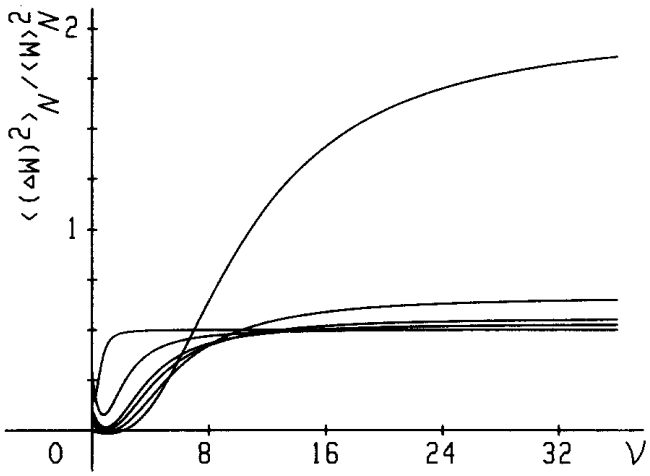

(*a*)

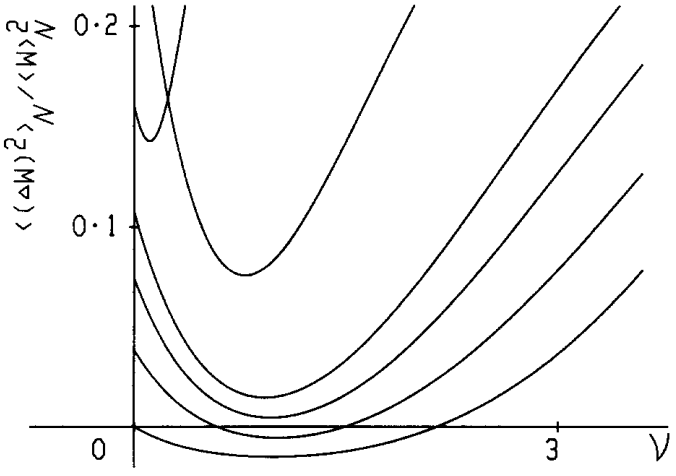

(*b*)

Figure 11. Dependence of the second reduced factorial moments $\langle(\Delta W)^2\rangle_{\mathcal{N}}/\langle W\rangle^2_{\mathcal{N}}$ for $|\beta, m\rangle_g$ with $m = 0$–$3, 10, 500$, $\alpha_0 = 7$ on the squeezing parameter v. Curves are ordered at the point $v = 4$ with $m = 0$–$3, 10, 500$ and (*b*) is a detail of the anti-bunching behaviour from (*a*).

respectively results in a differential equation

$$\dot{p}_n(t)=\tfrac{1}{2}\gamma[2(n-1)p_{n+1}(t)-2np_n(t)+\gamma\bar{n}[np_{n-1}(t)+(n+1)p_{n+1}(t)-(2n+1)p_n(t)], \tag{6.4}$$

which can be rewritten into difference equations. We solved (6.4) numerically.

An example for $m=3$, $v=1$, $\alpha_0=3$, $\bar{n}=1$, $gt_1=16\times10^{-4}$ (the first curve) and $(gt)_{i+1}=(gt)_i\times2$ is presented in figure 12. All structures in $p(n)$ are gradually smoothed out and it approaches the Bose–Einstein distribution of the reservoir.

Damped moments can be found analytically by the Heisenberg–Langevin method [12]. The explicit solutions, holding for all initial moments, result after some simple calculations:

$$\left.\begin{aligned}
\langle a(t)\rangle &= \langle a(0)\rangle\exp(-\gamma t/2)=\langle a^+(t)\rangle^*,\\
\langle a^2(t)\rangle &= \langle a^2(0)\rangle\exp(-\gamma t)=\langle a^{+2}(t)\rangle^*,\\
\langle a^+(t)a(t)\rangle &= \langle n(t)\rangle=\langle n(0)\rangle\exp(-\gamma t)+\bar{n}(1-\exp(-\gamma t)),\\
\langle\Delta^2 n\rangle &= \langle n^2(t)\rangle-\langle n(t)\rangle^2\\
&= \langle\Delta^2 n(0)\rangle\exp(-2\gamma t)+\langle n(0)\rangle(2\bar{n}+1)\times\exp(-\gamma t)\\
&\quad\times[1-\exp(-\gamma t)]+\bar{n}^2[1-\exp(-\gamma t)]^2+\bar{n}[1-\exp(-\gamma t)],\\
\left\langle\left(\Delta_p^q(t)\right)^2\right\rangle &= 1+\left[\left\langle\left(\Delta_p^q(0)\right)^2\right\rangle-1\right]\exp(-\gamma t)+2\bar{n}[1-\exp(-\gamma t)].
\end{aligned}\right\} \tag{6.5}$$

The unknown moments for $t=0$ are in (2.13)–(2.16). Moments from (6.5) agree with those from (5.10), in the special limits chosen there, and with the results in [14] for the states $|\beta,0\rangle_g$. Examples of the damped second reduced factorial moments for the same parameters as in figure 11 (*a*) except $gt=3$ and $\bar{n}=3$ as in figure 13. In the course of evolution, curves reordered themselves conversely to figure 11 (*a*), so that it is obvious that damping does not apply too much of the second reduced factorial moment for higher Fock states.

Finally we point out that we can find other moments by integrating the elements $\langle n|\rho a^{+i}|n\rangle$ in the same way as the photon-number distributions in (6.4). We will not go into details here, but show several examples of such calculations in figures 15–16.

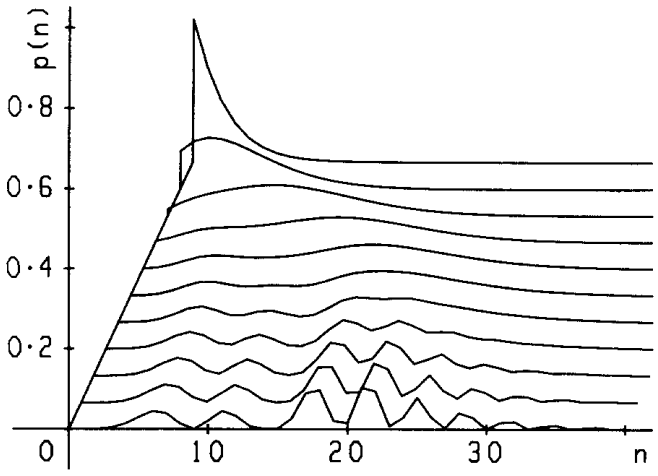

Figure 12. Time evolution of the photon-number distribution $p(n)$ for damping of the state $|\beta,m=3\rangle_g$ with $m=3$, $v=1$, $\alpha_0=3$ and $\bar{n}=1$. The nearest curve corresponds to $gt_1=16\times10^{-4}$ and the following curves to $gt_{i+1}=2gt_i$.

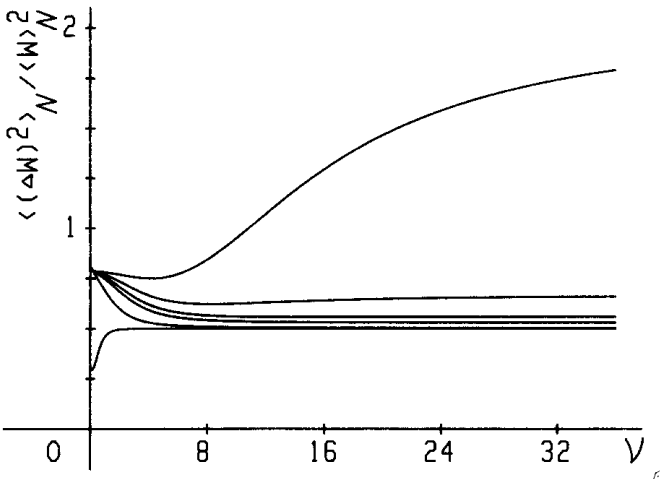

Figure 13. Dependence of the second reduced factorial moments on ν for damping of the states $|\beta, m\rangle_g$. The initial parameters are as in figure 11 and damping parameters are $gt=3$, $\bar{n}=3$. Curves are reordered conversely to those in figure 11.

6.3. *Two-photon damping*

An interesting situation arises for multiphoton absorptions [7]. The corresponding generalized master equations (5.2) all acquire a similar structure. For a two-photon case we show evolution of the photon-number statistics in figure 14 under the same conditions as in figure 12 for the usual damping, with the only changes that $gt_1=10^{-4}$ and $\bar{n}=0$. The present curves look sharper, which reflects the fact that a two-photon absorption can narrow the photon-number statistics [7].

Figure 15 (*a*) represents evolution of the corresponding reduced photon-number variance $\langle(\Delta n)^2\rangle/\langle n\rangle$ for $m=0$, $\alpha_0=3$, $\nu=0$–$0{\cdot}6$ (ν grows from the *upper* curve) and $gt=0$–$0{\cdot}04$. Continuation for $\nu=0{\cdot}8$–$1{\cdot}4$ is shown in figure 15 (*b*) (ν grows from the *lower* curve). The curves look like having a common limit value for $gt\to\infty$, which is perhaps true, at least for curves starting from sub-Poissonian states. A consequence of this fact is that the statistics of the curves with an input photon-number variance

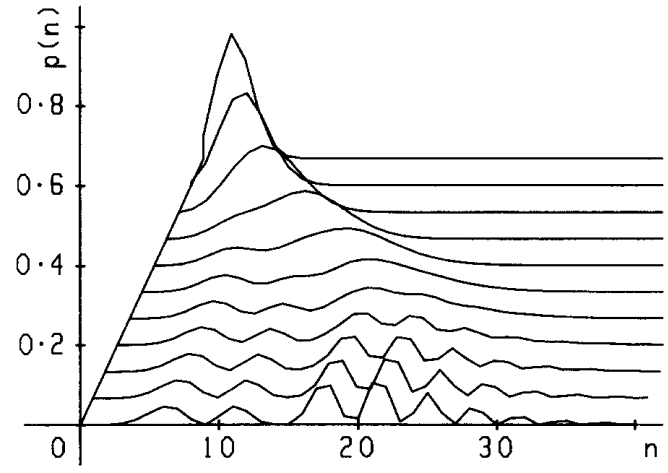

Figure 14. Time evolution of the photon-number statistics $p(n)$ for two-photon damping of the state $|\beta, m=3\rangle_g$ under initial conditions as in figure 12 with the only changes $\bar{n}=0$ and $gt_1=10^{-4}$.

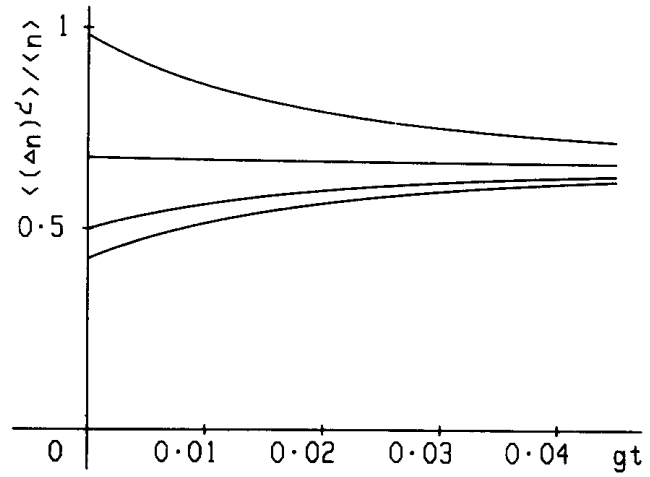

(*a*)

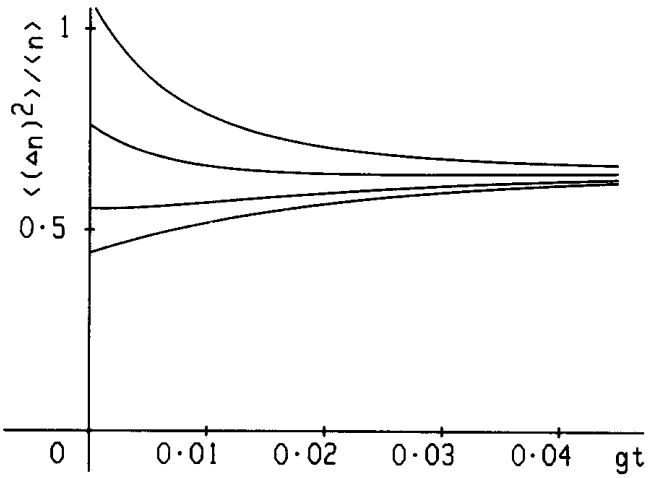

(*b*)

Figure 15. Time evolution of the reduced photon-number variance $\langle(\Delta n)^2\rangle/\langle n\rangle$ for a two-photon damping of the state $|\beta, m\rangle_g$ with $m=0$, $\alpha_0=3$, $\nu=0$–$0{\cdot}6$ corresponds to (*a*) (ν grows from the upper curve). Figure 15 (*b*) is a continuation for $\nu=0{\cdot}8$–$1{\cdot}4$ (ν grows from the lower curve).

under such a hypothetical limit only become broader. Analogous results appear in the first paper of [2].

Figure 16 finally displays evolution of the coordinate quadratures (5.9) ($\omega=\hbar/2=1$ is chosen) for the conditions in figure 15 (*a*) (the bottom curves, where ν grows down, hold for $\langle(\Delta q)^2\rangle$ and the opposite is true for $\langle(\Delta p)^2\rangle$). The curves are now monotonously ordered with increasing ν, which holds for all values of ν. Similar results can be found for higher photon damping.

7. Conclusion

We have investigated displaced and squeezed Fock states as a generalization of TCSs [8]. The general approach to generating functions permitted us to find all the important functions for analytical investigations of the states $|\beta, m\rangle_g$. Interesting

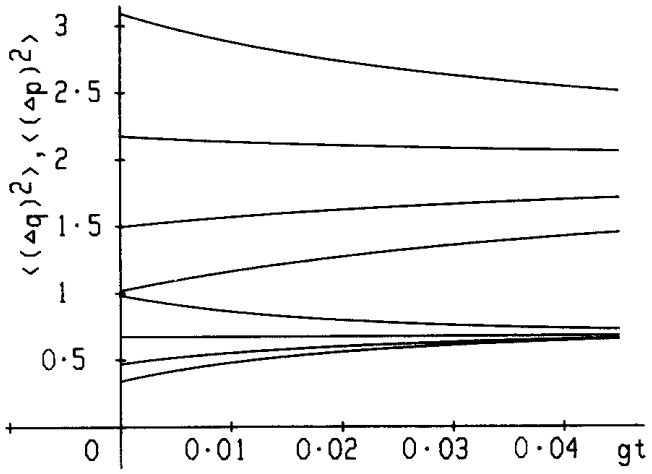

Figure 16. Time evolution of the coordinate quadratures $\langle(\Delta q)^2\rangle$, $\langle(\Delta p)^2\rangle$ for two-photon damping of the state $|\beta, m\rangle_g$ with the initial conditions as in figure 15 (*a*) ($\omega=\hbar/2=1$ is chosen; the bottom curves, on which ν grows down, hold for $\langle(\Delta q)^2\rangle$ and the opposite is true for $\langle(\Delta p)^2\rangle$).

behaviour of their quasi-distributions and photon-number distributions was observed. We found that $\phi_{\mathscr{A}}$, for a given $|\beta, m\rangle_g$ and $|\nu|$ not too small, is not continuous. This prompted us to think that new quantum phenomena could be disclosed when these states are used as the input of a suitable process. We can imagine that the disconnected parts of $\phi^m_{\mathscr{A}}$ could serve as relatively independent parts of the mode. In subsequent investigations we studied $|\beta, m\rangle_g$ states as the input of the Kerr nonlinear medium [4]. A lot of interesting results have been found, which will be published [21].

We have also used these states as an input in the Jaynes–Cummings Hamiltonian [22] for one-photon case $\sigma^+ a$, two-photon degenerate case $\sigma^+ a^2$, non-degenerate case $\sigma^+ a_1 a_2$ and three-photon case $\sigma^+ a_1^2 a_2$. In all these cases it could be seen that the chaotic Rabi oscillations of the atom disappear with a narrowing of the statistics of the modes.

We would like to draw attention to the fact that $|\beta, m\rangle_g$ states form a special basis of squeezed states which might find their application when general squeezed states are studied. We note that by applying the operators a^{+i} from the left and a^i from the right of the transformed completeness relation (3.15)

$$\int S(\zeta)D(\beta)|0\rangle\langle 0|D^+(\beta)S^+(\zeta)\frac{\mathrm{d}\beta^2}{\pi}=1,$$

and using (2.8) and (2.9) for commutation of a^+, and a with $S(\zeta)D(\beta)$, and $S(\zeta)^+D(\beta)^+$ respectively, we obtain interesting representations of the operators $a^{+i}a^i$. $|\beta, m\rangle_g$ may be important not only in optics, but also, for example, in molecular or solid state physics. There, in elementary versions, some quasi-particle modes with finite damping rate could be found in damped states $|\beta, m\rangle_g$.

Acknowledgments

The author would like to thank Dr J. Peřina for his stimulating discussions, Dr A. Lukš for his discussions concerning quasi-distributions and wavefunctions and Dr Z. Hradil for his helpful comments on this paper.

Appendix

If we use the Baker–Hausdorff identity [12],

$$\begin{aligned}\exp(A+B)&=\exp(A)\exp(B)\exp\{-[A,B]/2\}\\&=\exp(B)\exp(A)\exp\{[A,B]/2\},\end{aligned}\tag{A 1}$$

where A, B are non-commuting operators fulfilling

$$[B,[A,B]]=[A,[A,B]]=0,$$

and the matrix element $\langle\alpha|\beta\rangle_g$ from [8]

$$\langle\alpha|\beta\rangle_g=\frac{1}{\sqrt{\mu}}\exp\left[-\frac{|\alpha|^2}{2}-\frac{|\beta|^2}{2}-\left(\frac{\nu}{2\mu}\right)\alpha^{*2}+\left(\frac{\nu^*}{2\mu}\right)\beta^2+\frac{1}{\mu}\alpha^*\beta+i\theta\right],\tag{A 2}$$

we obtain

$$\begin{aligned}&\langle\alpha|S(\zeta)D(\beta)\exp(\lambda a^+)|0\rangle=\langle\alpha|S(\zeta)\exp[\lambda(a^+-\beta^*)]\,D(\beta)|0\rangle\\&=\exp(-\lambda\beta)\langle\alpha|S(\zeta)\exp(\lambda a^+)\exp(-|\beta|^2/2)\exp(\beta a^+)\exp(-\beta^* a)|0\rangle\\&=\exp\left(-\lambda\beta-\frac{|\beta|^2}{2}\right)\langle\alpha|S(\zeta)\exp[(\lambda+\beta)a^+]|0\rangle\\&=\exp\left(-\lambda\beta^*-\frac{|\beta|^2}{2}+\frac{|\lambda+\beta|^2}{2}\right)\langle\alpha|S(\zeta)D(\lambda+\beta)|0\rangle\\&=\frac{1}{\sqrt{\mu}}\exp\left(-\lambda\beta^*-\frac{|\beta^2|}{2}-\frac{|\alpha^2|}{2}-\frac{\nu}{2\mu}\alpha^{*2}+\frac{\nu^*}{2\mu}(\lambda+\beta)^2+\frac{\alpha^*}{\mu}(\lambda+\beta)+i\theta\right)\\&=\exp\{\lambda^2(\nu^*/2\mu)+\lambda[\beta(\nu^*/\mu)-\beta^*+\alpha^*/\mu]\}\langle\alpha|\beta\rangle_g\\&=\exp\{\lambda^2(\nu^*/2\mu)+\lambda(\alpha^*-\alpha_0^*)/\mu\}\langle\alpha|\beta\rangle_g\\&=\exp\{\lambda^2 A+\lambda B\}\langle\alpha|\beta\rangle_g\\&=\exp(-B^2/4A)\exp\{A(\lambda+B/2A)^2\}\langle\alpha|\beta\rangle_g,\end{aligned}\tag{A 3}$$

where we took into account (2.8), (2.2), (2.4), (2.7) and (A 1). Now we employ the definition of the Hermite polynomials [17]

$$H_n(z)=(-1)^n\exp(z^2)\frac{d^n}{dz^n}\exp(-z^2),\tag{A 4}$$

and make the substitution $z=-(-A)^{1/2}(\lambda+B/2A)$ in (A 3). This choice is more convenient than the other possible $z=(-A)^{1/2}(\lambda+B/2A)$, which can easily lead, when badly treated, to serious errors.

We can continue as follows

$$\langle\alpha|S(\zeta)D(\beta)|m\rangle=\frac{1}{\sqrt{m!}}\frac{\partial^m}{\partial\lambda^m}\langle\alpha|S(\zeta)D(\beta)\exp(\lambda a^+)|0\rangle\Big|_{\lambda=0}$$

$$=\langle\alpha|\beta\rangle_g\frac{1}{\sqrt{m!}}$$

$$\times\exp(-B^2/4A)(-\sqrt{-A})^m\frac{\mathrm{d}^m}{\mathrm{d}z^m}\Big|_{\lambda=0}\exp(-z^2)$$

$$=\frac{1}{\sqrt{m!}}\langle\alpha|\beta\rangle_g(\sqrt{-A})^m H_m(z)\Big|_{\lambda=0}, \tag{A 5}$$

from which $\phi^m_{\mathscr{A}}$ directly results

$$\phi^m_{\mathscr{A}}(\alpha)=\frac{1}{\pi m!}|v^*/2\mu|^m\left|H_m\left(\frac{\alpha^*-\alpha_0^*}{(-2\mu v^*)^{1/2}}\right)\right|^2|\langle\alpha|\beta\rangle_g|^2. \tag{A 6}$$

Similarly, using the matrix element $\langle n|\beta\rangle_g$ found in [8]

$$\langle n|\beta\rangle_g=\frac{1}{(m!\mu)^{1/2}}\left(\frac{v}{2\mu}\right)^{n/2}H_n\left(\frac{\beta}{(2\mu v)^{1/2}}\right)\exp\left(-\frac{|\beta|^2}{2}+\frac{v^*}{2\mu}\beta^2\right). \tag{A 7}$$

we obtain

$$\langle n|S(\zeta)D(\beta)\exp(\lambda a^+)|0\rangle=\exp\left(-\lambda\beta^*-\frac{|\beta|^2}{2}+\frac{|\lambda+\beta|^2}{2}\right)\langle n|S(\zeta)D(\lambda+\beta)|0\rangle$$

$$=\frac{1}{(n!\mu)^{1/2}}\left(\frac{v}{2\mu}\right)^{n/2}H_n\left(\frac{\beta+\lambda}{(2\mu v)^{1/2}}\right)\exp\left[-\frac{|\beta|^2}{2}+\left(\frac{v^*}{2\mu}\right)\beta^2\right]$$

$$\times\exp\left[\lambda^2\left(\frac{v^*}{2\mu}\right)+\lambda\left(\frac{v^*}{\mu}\beta-\beta^*\right)\right]. \tag{A 8}$$

Therefore

$$\langle n|\beta,m\rangle_g=\frac{1}{\sqrt{m!}}\frac{\partial^m}{\partial\lambda^m}\langle n|S(\zeta)D(\beta)\exp(\lambda a^+)|0\rangle\Big|_{\lambda=0}$$

$$=\frac{1}{(n!m!\mu)^{1/2}}\left(\frac{v}{2\mu}\right)^{n/2}\exp\left[-\frac{|\beta|^2}{2}+\left(\frac{v^*}{2\mu}\right)\beta^2\right]$$

$$\times\sum_{i=0}^{\min(m,n)}\binom{m}{i}2^i\frac{n!}{(n-i)!}\left(\frac{1}{(2\mu v)^{1/2}}\right)^i H_{n-i}\left(\frac{\beta}{(2\mu v)^{1/2}}\right)$$

$$\times\left[\left(-\frac{v^*}{2\mu}\right)^{(m-i)/2}\right]H_{m-i}\left[-\frac{\alpha_0^*}{(-2\mu v^*)^{1/2}}\right], \tag{A 9}$$

where we followed the way from (A 3) to (A 5) with new coefficients A and B and used for formula

$$\frac{\mathrm{d}}{\mathrm{d}z}H_n(z)=2nH_{n-1}(z). \tag{A 10}$$

References

[1] SLUSHER, R. E., YURKE, B., GRANGIER, P., LAPORTA, A., WALLS, D. F., and REID, M., 1987, *J. opt. Soc. Am.* B, **4,** 1453 and following articles.

[2] KÁRSKÁ, M., and PEŘINA, J., 1990, *J. mod. Optics*, **37,** 195; PEŘINOVÁ, V., and LUKŠ, A., 1988, *J. mod. Optics*, **35,** 1513 and references therein.

[3] D'ARIANO, G. M., and STERPI, N., 1989, *Phys. Rev.* A, **39,** 1860.

[4] KITAGAVA, M., and YAMAMOTO, Y., 1986, *Phys. Rev.* A, **34,** 3974.

[5] FILIPOWITZ, P., JAVANAINEN, J., and MEYSTRE, P., 1986, *J. opt. Soc. Am.* B, **3,** 906; WATANABE, K., and YAMAMOTO, Y., 1988, *Phys. Rev.* A, **38,** 3566; KRAUSE, J., SCULLY, M. O., WALTHER, T., and WALTHER, H., 1989, *Phys. Rev*, A, **39,** 1915; HOLMES, C. A., MILBURN, G. J., and WALLS, D. F., 1989, *Phys. Rev.* A, **39,** 2493.

[6] HONG, C. K., and MANDEL, L., 1986, *Phys. Rev. Lett.*, **56,** 58.

[7] PEŘINA, J., 1984, *Quantum Statistics of Linear and Nonlinear Optical Phenomena* (Dordrecht: D. Reidel); GLAUBER, R. J., 1970, *Quantum Optics*, edited by S. M. Kay and A. Maitland (London: Academic).

[8] YUEN, H. P., 1976, *Phys. Rev.* A, **13,** 2226.

[9] BISHOP, R. P., and VOURDAS, A., 1987, *J. Phys.* A, **20,** 3743.

[10] LUKŠ, A., PEŘINOVÁ, V., and PEŘINA, J., 1988, *Optics Commun.*, **67,** 149.

[11] LOUDON, R., and KNIGHT, P. L., 1987, *J. mod. Optics*, **34,** 710.

[12] LOUISELL, W. H., 1973, *Quantum Statistics Properties of Radiation* (New York: Wiley).

[13] SCHLEICH, W., and WHEELER, J. A., 1987, *J. opt. Soc. Am.* B, **4,** 1715.

[14] PEŘINOVÁ, V., KŘEPELKA, J., and PEŘINA, J., 1986, *Optica Acta*, **33,** 1263.

[15] PEŘINOVÁ, V., 1981, *Optica Acta*, **28,** 747.

[16] RAI, J., and MEHTA, C. L., 1988, *Phys. Rev.* A, **37,** 4497.

[17] MESSIAH, A., 1985, *Quantum Mechanics I*, (Amsterdam: North-Holland); LEBEDEV, N. N., 1965, *Special Functions and their Applications* (Englewood-Cliffs, New Jersey: Prentice-Hall).

[18] CARRUTHERS, D., and NIETO, M. M., 1965, *Phys. Rev. Lett.*, **14,** 387; CAHILL, K. E., and GLAUBER, R. J., 1969, *Phys. Rev.*, **177,** 1857.

[19] AGARWAL, G. S., and ADAM, G., 1989, *Phys. Rev.* A, **39,** 6259.

[20] KIM, M. S., DE OLIVEIRA, F. A. M., and KNIGHT, P. L., 1989, *Optics Commun.*, **72,** 99; the same subject appeared in 1989, *Coherence and Quantum Optics 6*, edited by J. H. Eberly, L. Mandel and E. Wolf (New York: Plenum) and will be published in *Phys. Rev.*

[21] KRÁL, P., 1990, *Phys. Rev.* A (submitted).

[22] JAYNES, E. T., and CUMMINGS, F. W., 1963, *Proc. Inst. Radio Engrs*, **51,** 83.